A NUMERICAL INVESTIGATION OF THE EFFECT OF PERFORATED PINS AND CONE INCLINATION ANGLE ON THE PERFORMANCE OF HEAT SINKS

2023
MASTER THESIS
MECHANICAL ENGINEERING

Mohammed Ahmed AL KAROOSHI

Thesis Advisor
Assist. Prof. Dr. Khaled M. N. CHAHROUR

A NUMERICAL INVESTIGATION OF THE EFFECT OF PERFORATED PINS AND CONE INCLINATION ANGLE ON THE PERFORMANCE OF HEAT SINKS

Mohammed AL KAROOSHI

Thesis Advisor
Assist. Prof. Dr. Khaled M. N. CHAHROUR

T.C.
Karabuk University
Institute of Graduate Programs
Department of Mechanical Engineering

Prepared as
Master Thesis

KARABÜK
July 2023

I certify that in my opinion the thesis submitted by Mohammed AL KAROOSHI titled “A NUMERICAL INVESTIGATION OF THE EFFECT OF PERFORATED PINS AND CONE INCLINATION ANGLE ON THE PERFORMANCE OF HEAT SINKS” is fully adequate in scope and in quality as a thesis for the degree of Master of Science.

Assist. Prof. Dr. Khaled M. N. CHAHROUR .....
Thesis Advisor, Department of Mechanical Engineering

This thesis is accepted by the examining committee with a unanimous vote in the Department of Department of Mechanical Engineering as a Master of Science thesis. 03/07/2023

Examining Committee Members (Institutions)	Signature
Chairman : Assist. Prof. Dr. Abdulrazzak AKROOT (KBU)	.....
Member : Assist. Prof. Dr. Khaled M. N. CHAHROUR (KBU)	.....
Member : Assist. Prof. Dr. Wissam Hashim KHALIL (BU)	.....

The degree of Master of Science by the thesis submitted is approved by the Administrative Board of the Institute of Graduate Programs, Karabuk University.

Prof. Dr. Müslüm KUZU .....
Director of the Institute of Graduate Programs

This thesis contains information that I have gathered and presented in a manner that is consistent with academic regulations and ethical principles, and I affirm that I have appropriately cited any and all sources that are not my own work.

Mohammed Ahmed AL KAROOSHI

ABSTRACT

M. Sc. Thesis

A NUMERICAL INVESTIGATION OF THE EFFECT OF PERFORATED PINS AND CONE INCLINATION ANGLE ON THE PERFORMANCE OF HEAT SINKS

Mohammed Ahmed AL KAROOSHI

Karabük University
Institute of Graduate Programs
The Department of Mechanical Engineering

Thesis Advisor:
Assist. Prof. Dr. Khaled M. N. CHAHROUR
July 2023, 58 pages

Over the past few decades, researchers have shown significant interest in enhancing the thermal efficiency of heat sinks while simultaneously increasing the power generation capacity of electronic devices and reducing their size. Since industrial devices generate heat as a byproduct of power dissipation, which can impair their performance, a set of temperature limit constraints is necessary for nearly all these devices to function properly. That is, if overheating causes certain constraints to be exceeded, these engineering devices may malfunction in some way. As a result, heat sinks can be used to cool crucial components in a variety of significant applications, including computers, nuclear reactors, aviation engines, and data center server racks, in addition to a number of other microelectronic devices. Air cooling is the most widely used cooling method for heat dissipation in electronic thermal control. The key advantages of this cooling technology include decreased cost, convenience of design, easier access to air, and greater reliability.

In this study, conical perforated pin heat sinks were designed with multiple perforations (N = 0, 1, 2 and 3) and various conical pins at various inclination angles (Φ = 0°, 1°, 2° and 3°). The study aimed to investigate the effects of a perforated conical pin and cone inclination angle on heat transfer, pressure drop, CPU temperature, and hydrothermal performance (HTP) across the heat sinks using a 3D, turbulent flow, and a thermal conjugate model. A validated CFD model was employed to conduct a parametric analysis of the effects of the quantity and placement of circular holes. A summary of the results reveals that Model B3 exhibited the highest HTP value, reaching approximately 1.15 at U = 10m/s, with a commendable reduction in its heat sink mass of over 12%. Ultimately, the perforated conical pin heat sink demonstrates the potential to fulfil the primary objective of this investigation, namely achieving an overall improvement in Nusselt number, CPU temperature, pressure drop, and reduced heat sink mass.

Keywords **:** Conical pin heat sink, Perforated conical pins, k-ω SST model, Conjugate heat transfer.

Science Code : 91411

ÖZET

M. Sc. Thesis

DELİKLİ PİMLERİN VE KONİ EĞİM AÇISININ ISI ALICININ PERFORMANSI ÜZERİNDEKİ ETKİSİNİN SAYISAL İNCELENMESİ

Mohammed Ahmed AL KAROOSHI

Karabük Üniversitesi
Lisansüstü Eğitim Enstitüsü
Makine Mühendisliği Anabilim Dalı

Tez Danışmanı:
Dr. Öğr. Üyesi Khaled M. N. CHAHROUR
Temmuz 2023, 58 sayfa

Geçtiğimiz birkaç on yıl boyunca araştırmacılar, ısı alıcılarının termal verimliliğini artırmaya, aynı zamanda elektronik cihazların güç üretim kapasitesini artırmaya ve boyutlarını küçültmeye büyük ilgi göstermişlerdir. Endüstriyel cihazlar, güç dağıtımının bir yan ürünü olarak ısı ürettiğinden ve bu da performanslarını olumsuz etkileyebileceğinden, bu uygulamaların neredeyse tamamının düzgün çalışabilmesi için bir dizi sıcaklık sınırı kısıtlaması gereklidir. Yani, aşırı ısınma belirli kısıtlamaların aşılmasına neden olursa, bu mühendislik cihazları bir şekilde arızalanabilir. Sonuç olarak, ısı alıcıları bilgisayarlar, veri merkezi sunucu rafları ve diğer mikroelektronik cihazların yanı sıra havacılık motorları ve nükleer reaktörler de dahil olmak üzere çeşitli önemli uygulamalardaki kritik bileşenleri soğutmak için kullanılabilir. Hava soğutma, elektronik termal kontrolde ısı dağılımı için en yaygın kullanılan soğutma yöntemidir. Bu soğutma teknolojisinin temel avantajları arasında

düşük maliyet, tasarım kolaylığı, havaya daha kolay erişim ve daha fazla güvenilirlik yer almaktadır.

Bu çalışmada, konik delikli pimli ısı alıcıları çoklu delikler (N = 0, 1, 2 ve 3) ve çeşitli konik pim eğim açıları (Φ=0°, 1°, 2° ve 3°) ile tasarlanmıştır. Çalışma, delikli konik pim ve koni eğim açısının ısı alıcıları boyunca ısı transferi, basınç düşüşü, işlemci sıcaklığı ve hidrotermal performans (HTP) üzerindeki etkilerini 3 boyutlu (3B), türbülanslı akış ve termal eşlenik model kullanarak araştırmayı amaçlamıştır. Konik deliklerin miktarı ve yerleşiminin etkilerinin parametrik bir analizini yapmak için doğrulanmış bir Hesaplamalı Akışkanlar Dinamiği (HAD) modeli kullanılmıştır. Sonuçlar, B3 modelinin en yüksek HTP değerini sergilediğini, U = 10 m/s'de yaklaşık 1,15'e ulaştığını ve ısı alıcı kütlesinde %12'nin üzerinde övgüye değer bir azalma olduğunu göstermektedir. Sonuç olarak, delikli konik pimli ısı emici, bu araştırmanın birincil amacını yerine getirme potansiyelini göstermektedir; yani Nusselt sayısında, işlemci sıcaklığında, basınç düşüşünde ve azaltılmış ısı alıcı kütlesinde genel bir iyileşme sağlayabilmektedir.

Anahtar Kelimeler : Konik pimli soğutucu, elikli konik pimler, k-ω SST modeli, eşlenik ısı transferi.

Bilim Kodu **:** 91411

ACKNOWLEDGEMENT

In the beginning, Alhamdulillah. Allah is the first and last helper, and if it were not for His mercy, I would not have reached where I am now. Many thanks to my supervisor, Assist. Prof. Dr. Khaled M. N. CHAHROUR for all the information and recognition I got from him and for his endless support, understanding, and kindness. and I do not forget my teacher, Dr. Amer. Al DAMOOK has done a lot for me in my BA and MA. I am really happy and grateful to have the opportunity to be his student. I am grateful to my professor, Prof. Khalid M. Mousa, who gave me a lot of his time in proofreading this thesis, for him many thanks and praise. Finally, to those to whom I dedicate the fruits of my efforts to support me, my beautiful family, words of gratitude are not enough for you.

CONTENTS

Page

Page

Page

LIST OF FIGURES

Page

Page

LIST OF TABLES

Page

SYMBOLS AND ABBREVITIONS INDEX

SYMBOL

D_h	: Hydraulic diameter	m
A_s	: Surface area	m^2
A_p	: Projected base area	m^2
T	: Temperature	℃
T_{base}	: Base temperature	℃
$\dot{Q}_{conv}$	: Heat transfer convection	W
Q	: Power applied on the base	KJ
hp	: Projected heat transfer coefficient	$W/m^2 \cdot K$
h	: Heat transfer coefficient	$W/m^2 \cdot K$
K	: Thermal conductivity	$W/m \cdot K$
N_f	: Number of fins	-
D_f	: Fin diameter	mm
H_f	: Fin height	mm
Θ	: Hole diameter	mm
ϕ	: Angle of inclination of the cone	degree
S	: Distance between each pin	mm
W_c	: Channel width	mm
H_c	: Channel height	mm
H_b	: Height base heat sink	mm
W_b	: Width base heat sink	mm
C_p	: Heat capacity	J/kg·K
U	: Air velocity	m/s
ρ	: Fluid density	kg/m^3
μ	: Fluid viscosity	kg/m·s
Δp	: Pressure drop	Pa
Nu	: Nusselt number	-

Re	: Reynolds number	-
α	: Fluid thermal diffusivity	m^2/s
α, β, β^*	: Turbulence model constants	-
μ_t	: Turbulent eddy viscosity	kg/m·s
ν	: Kinematic viscosity	m^2 /s
νt	: Turbulent kinematic viscosity	m^2/s
ω	: k-ω Turbulence model constant	-

ABBREVIATIONS

PHS	: Pin heat sink	-
PFHSs	: Plate fin heat sinks	-
PPHS	: Perforated pin heat sink	-
CPU	: Central processing unit	-
CFD	: Computational fluid dynamics	-
HTP	: Hydrothermal performance	-
RANS	: Reynolds-Averaged Navier-Stokes	-
PDE	: Partial differential equation	-
FVM	: Finite volume method	-
GIT	: Grid independent test	-
SIMPLE	: Semi-Implicit Method for Pressure Linked Equations	-

PART 1

INTRODUCTION

1.1. INTRODUCTION

Because of the growing reliance on social media, education, business, transportation, and other areas of economic activity, information and communication technology (ICT) has evolved into our society's most valuable source of information and data [1]. It has now become essential to create data centers which are essential for digital factories to process, manage, store, and share information and data utilizing information and communication technology [2]. A data center can be divided into four primary parts: the power equipment, which can include batteries and power distribution items; the cooling equipment, which can include computer room air conditioning units; the information technology equipment, which can include storage, servers, and networks; and other elements, which can include light and fire safety systems [3]. Most data centers are composed of electronic elements that are used to organize data processing, storage, and transfer, these elements produce a great amount of heat, which needs to be removed from the electronic components of the data center at a rate that is instant enough to avoid major overheating troubles and faults in these electronic components [4] [5]. In a typical data center, the cost of IT equipment and cooling equipment is expected to be more than 30% of the total cost. As a result, the heat sink that is positioned above the CPU, as seen in Figure 1.1, is an essential component of a server [6].

In electronic devices, excessive heat can lead to the failure of mechanisms. Such heat can be caused by metal migration, the formation of voids, and the development of intermetallic compounds. In fact, the highest temperature at which such devices are able to function is one of the common factors that play a role in determining the dependability of electronic items. The rate at which these failures occur

approximately doubles for every 100℃ that is added over the critical working temperature of the high-power electronics, which is 85℃ [7]. Because of this, thermal management in electronic devices is of the utmost significance, as evidenced by marketing [8]. Another important point is the escalating price of thermal management products, which reached $8 billion in 2011, up from around $7.5 billion in 2010, and was expected to reach $10.9 billion by 2016. This was an annual growth rate of 6.4%. However, other essential cooling supplies such as software, interface materials, and substrates, only achieved 6% of the market [9]. Thermal management hardware components, fans, and heat sinks account for 84% of the market. Although a significant amount of research has been conducted on fluid movement in heat sinks and their thermal properties, there is still a lack of knowledge on heat sinks in general, particularly PHS. For this reason, researchers have pushed research into the design optimization and analysis of heat airflow proficiency via PPHS for use in electronic cooling systems.

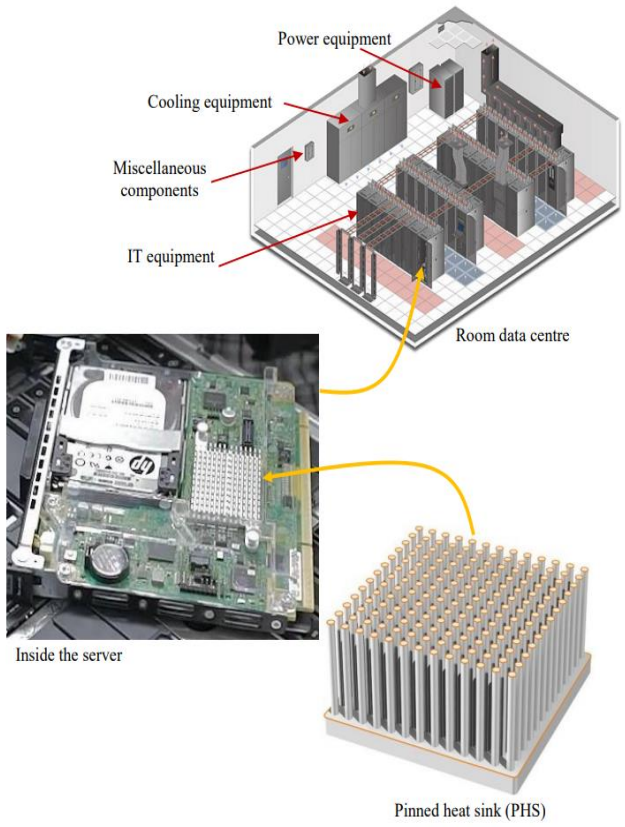

Figure 1.1. Data center infrastructure, server, and pinned heat sink [6].

1.2. INTRODUCTION TO HEAT SINK TECHNOLOGY

PFHS and PHS, also known as pinned heat sinks, are the second primary classifications of finned heat sinks, as shown in Figure 1.2 [10]. The heat sinks are designed and manufactured by many companies, some of which are Airedale in the United Kingdom and Raypak in the United States, to name just two examples. Copper and aluminum are two materials with elevated thermal conductivity and may be used to make heat sinks. The cost and ease of manufacture of heat sinks might vary depending on the type of heat sink material used. Heat sink technology, which is used for cooling electronics, has lately acquired popularity and reputation because it has a cheap start up cost, it is easy to install, and its production process is reliable [11]. In both the manufacturing process and the process of heat transmission, the characteristics of the fin shape perform an important role. The most typical geometries for homogeneous pin fins are rectangular, cylindrical, square, conical, elliptical, or quasi-conical forms. Other popular geometries are cylinder, square, and elliptical. Pins are also an effective way to create a high heat exchange region without an excessive main surface area in various appliances, such as the cooling of electronic equipment and procedures that utilize liquid coolants or gas. Furthermore, pins function as turbulence promoters, improving average heat exchange by breaking up the thermal boundary layer [12] [13] [14]. As a result, it is a perfect time to implement this technology in both industrial applications and traditional heat sinks. In general, pin fin layouts, consist of a grid of solid pins arranged directly on the surface of the heat sink. The pins in a pin array are often staggered or in line, and the flow of the working fluid can be perpendicular or parallel to the axis of the pin.

1.3. IMPORTANCE OF ELECTRONICS COOLING

Heat is typically produced as a by-product of power dissipation in engineering. If these devices become dangerously hot, it can cause failures in the underlying system. This is mostly due to the fact that virtually all applications are required to run within certain temperature ranges in order to perform correctly. At the moment, the thermal power losses that are caused by electronic equipment increase as their size reduces [8]. Many different types of industrial applications make use of forced

convection of heat sinks so that they can avoid the potentially disastrous impact of overheating. As a result, it is very necessary to take into consideration the cooling system for electrical elements. The primary manufacturing uses of heat sinks include the cooling of fuel components in nuclear reactors, as well as their use in small electronic devices, electronic boards and apparatuses, the central processing unit of personal computers and data centers, gas turbine blade ;coolant tracks, internal combustion engines, advanced electronic chips, electrical devices, aerospace production, and the cooling of electronic components [15, 16, 17]. Plate and pin fins find widespread application in cooling complex gas turbine blades, integrated chips found in electronic equipment, central processing units (CPUs) found in personal computers, and other electronic components [13] [18] [19]. To the best of the author's knowledge, fin punctures may play an important role in the thermal airflow that occurs via heat sinks. This means that they will enhance cooling performance while simultaneously reducing pressure drops. These heat sinks might be useful for cooling electrical devices and internal combustion engines, such as transformers, computer power supplies, and radiator fins, and so on.

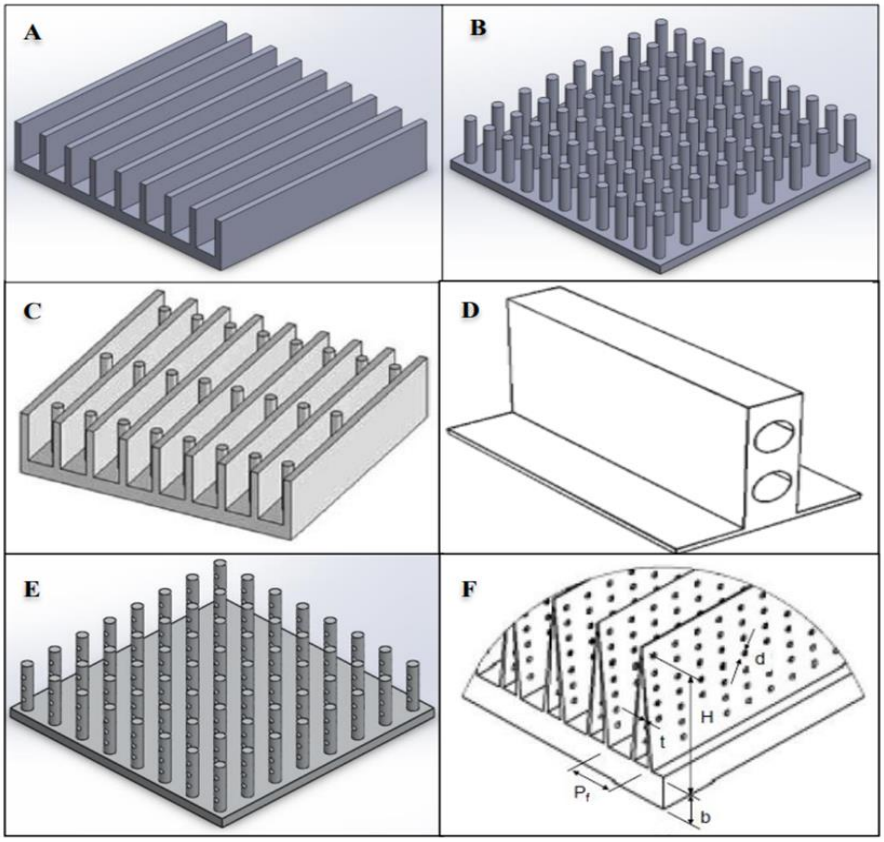

Figure 1.2. Different types of fin: (A) solid plate fins; (B) solid pins; (C) compact plate-pins; (D) perforated plate; (E) perforated pins; and (F) perforated folded fin heat sinks [10].

1.4. PROBLEM STATEMENT

The most crucial way to transport heat from an energy source to a fluid is the heat sink, which is drawing increased attention. Due to its fundamental nature in electronic equipment, it is frequently used in the cooling of thermal systems. Research on heat sinks began in the 1980s. The goal of the first study was to increase the rate of heat exchange by reducing the size of the heat sink to the micrometer range [20]. Since then, a great deal of research has been done to improve the thermal performance of heat sinks utilizing various methods. Researchers chose to use low flow rates because of the strong pressure gradients. However, if flow rates are decreased, the capacity of the fluid flow to remove heat from a given temperature increase is constrained. It is therefore crucial to improve the design of the heat sink, reduce the number of fins, and simultaneously replace them with pins to save substrate material and optimize cooling functioning in general. With the required

amount of time, the heat sink with base plate pins appears. However, the following issues are present with this technique:

- Impairment of heat exchange between the fins and the coolant fluid.
- High fan power consumption due to high pressure drops.
- High temperature of the CPU which sometimes leads to damage to the heat sink.

1.5. AIMS AND OBJECTIVES OF THE CURRENT STUDY

The primary goal of this study is a numerical analysis of various perforated and pinned heat sink configurations that are suggested to lower CPU temperature, increase the heat transfer amount, and reduce the power of the fan so as to overcome the pressure drop via pinned heat sinks. Then, to achieve the lowest CPU temperature and power of fan consumption via a heat sink, each design's ideal thermal airflow properties, such as the dimensions of the perforations, are evaluated. Since convective heat transfer to the air as it flows via a grid of fins is also the most popular method of cooling microelectronics due to its low cost, relatively simple structure, availability, and ease of manufacturing, the specifications of pinned heat sinks are also stated for active air-cooling of electronic systems. Finally, employing cone fins and perforations will make these heat sinks lower in weight. This thesis will examine many forms of pin fin heat sinks, including designed four cone fin pins, each with a different inclination angle.

Below are the objectives of the current study:

- To study the effect of increasing the number of fin holes and the angle of inclination of the conical fins on heat sink performance.
- To increase heat exchange by increasing the Nusselt number.
- To reduce pressure drops so as to reduce energy consumption.
- To raise heat sink efficiency by reducing CPU temperature.
- To reduce the mass of the heat sink by perforating the fins and raising the angle of inclination of the cone fins.

1.6. THESIS STRUCTURE

This part provides a simplified explanation of the main parts of the current study.

Part 1 provides an introduction to the refrigeration mechanism, its importance in modern technology, and the research problem and objectives.

Part 2 explains the heat sink, its types, heat transfer, and the characteristics of flow in addition to the types of boundary layers.

Part 3 presents an extensive literature review of relevant research, specifically the experimental and numerical development of perforated fins.

Part 4 presents the numerical model preparation, assumptions, governing equations and boundary conditions, and validation, including various parameters and their impact on heat sink performance reported in detail.

Part 5 presents the modeling results of the different models that have been developed and compares and discusses the results with relevant previous research.

Part 6 is the conclusion of this study and contains a summary and suggestions for possible future research.

PART 2

THERMAL-HYDRAULIC IN HEAT SINKS BACKGROUND

2.1. HEAT SINK

A heat sink is a material or device that absorbs or distributes heat, particularly unwanted heat, and is one of the most often used approaches to cooling electronics systems. Excess thermal energy is dissipated via heat sinks. They are typically constructed of aluminum and copper, but because copper is more expensive, they are rarely utilized. Figure 2.1 shows an example of a heat sink [21].

The heat sink works with Pelletier cells or heat pipes as part of an integrated cooling system. Hybrid solutions are utilized when the performance of a heat sink is insufficient, such as combining it with active cooling systems like fans. This necessitates the use of forced air circulation because there is barely a temperature differential between the heat sink and surrounding air. Heat sinks operate silently and without the need for electricity, and they do not have any moving parts that can break down with time. The largest flaw with highly heated sensitive components is typically a lack of cooling power, which may be overcome by having enough airflow through the heat sink. Despite being viewed as a remedy for the prior flaw, this procedure has drawbacks. The volume of the heat sink must be inordinately large and consequently heavy to carry out its function because it necessitates the addition of fans and other equipment with a higher degree of unreliability.

Figure 2.1. Example of a heat sink [21].

2.2. SOLID PINNED HEAT SINKS

Even though PFHSs have been the subject of numerous optimization studies, these studies have not been able to overcome the inherent limitation caused by the parallel plate arrangement. This arrangement prevents air from flowing over the heat sink channels smoothly, forming a boundary layer and lowering the average feasible heat exchange. Even though PFHS has been the subject of numerous optimization studies, these studies have not been able to overcome this inherent limitation. PFHSs may be effectively replaced with PHSs, which prevents the creation of the thermal boundary layer on efficient surfaces. This layer is accountable for limiting the value of heat exchange achieved by plate fin designs. PHSs are an effective heat exchange solution. PHSs serve an important purpose as turbulence promoters that boost heat transfer rates. They accomplish this by disrupting the boundary layer with a larger ΔP than PFHSs. The ΔP and heat exchange rates of PHSs are significantly greater than those of PFHSs. In addition, PHSs have lower thermal resistance and average temperatures than PFHSs [22]. Figure 2.2 shows an example of a PHS.

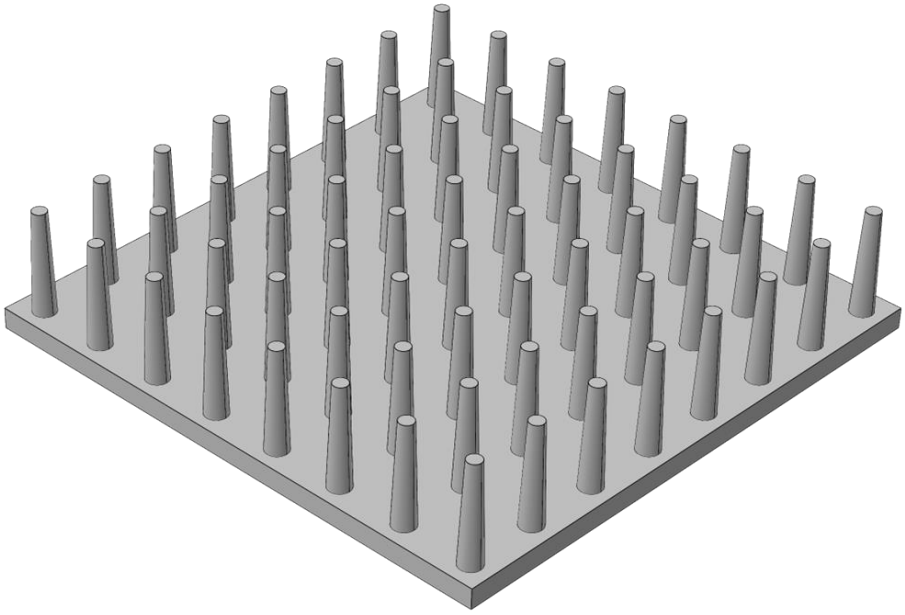

Figure 2.2. Heat sink with solid pins.

2.3. PERFORATED PINNED HEAT SINKS

The impact of perforations on the average heat exchange and the ΔP in PPHS has only been the focus of a relatively small number of studies. Pin punctures offer considerable advantages by improving heat transmission, reducing ΔP through the heat sink, and decreasing the power required to drive the fan. These holes make it possible to reduce the weight of the PHS. Figure 2.3 shows two different variants of these punctures: single and multiple [23].

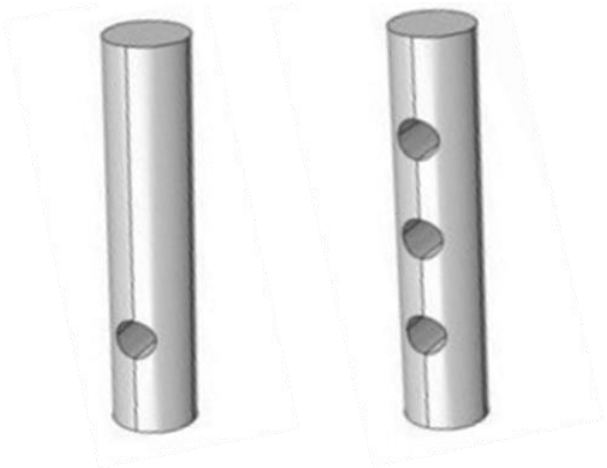

Figure 2.3. Single hole and multiple holes [23].

2.4. PHYSICAL MECHANISM OF CONVECTION HEAT TRANSFER

Both conduction and convection are ways that heat may be transmitted through fluids (through either liquids or gases), but which one is used depends on whether or not there is bulk fluid motion. Figures 2.4a and 2.4b show how convection occurs when there is motion in most of the fluid. Figure 2.4c shows how conduction occurs when there is very little motion in the fluid.

In practice, heat conduction and the movement of fluids are both essential components of the convective transmission of heat. Through the process of conduction, heat is transported from a hot surface to the closest layer of cooler fluid, and from there, this heat is transferred to the following layer of colder fluid through fluid motion, and so on. Because of this, the pace at which heat is transferred by convection is significantly quicker than the rate at which it is transferred via conduction [24].

Experience has shown that the dynamic viscosity of the fluid, the density of the fluid, the thermal conductivity of the fluid, the thermal capacity of the fluid, and the fluid velocity all influence convection heat transfer. Furthermore, it depends on the geometry, the kind of fluid flow, and the roughness of the solid surface. Because of this, the mechanism of heat transmission by convection is rather complex. The rate of heat exchange by convection quickens whenever there is a greater temperature disparity between a cold fluid and a hot surface. This rate can be specified with the help of Newton's law of cooling, thus:

$$\dot{Q}_{conv} = hA_s(T_s - T_\infty) \tag{2.1}$$

where h is the convective heat transfer coefficient, A_s the surface area, T_s the surface temperature, and T_∞ the ambient fluid temperature.

2.5. BASIC CONCEPT OF FLUID FLOW TYPES

Because the mechanics of fluids additionally have an impact on the process of convection heat exchange, this section will discuss the most common forms of fluid flow to better explain how fluid flow behavior influences the convection heat exchange process [24].

2.5.1. Viscous and Inviscid Flow

Viscous flow is the term utilized when the viscosity of a fluid is considered, and it is determined that the viscosity has a significant influence because of the fluid's internal flow opposition. Although a flow that is assumed to have no viscosity is called an inviscid flow, in other flows the effects of viscosity are so insignificant that they may be disregarded.

2.5.2. Internal and External Flow

External flow is a fluid driven above an item without being confined by the element's neighboring surfaces. Internal flow is the required passage of fluid through a pipe, duct, or other surface constrained channel.

2.5.3. Compressible and Incompressible Flow

Compressible flows are gas flows with significant changes in fluid density. Compressible flow is important in motors, aircraft, rockets, and jet engines, and similar items. Because liquid densities are for the most part steady, the flow is categorized as incompressible. Airflows are typically considered incompressible flows when the flow speed is sufficiently low.

2.5.4. Laminar and Turbulent Flow

Laminar flow is described as the parallel flow of a fluid with uniform smooth streamlines and ordered flow that does not interact with the fluid flow layers if we

take into consideration a fluid flow with extreme viscosity and low speed. Turbulent flows, on the other hand, are not required and involve irregular variations in local fluid velocity that generate a disarrangement between the fluid layers. The shift from laminar to completely turbulent fluid flow is described as transient fluid flow. These flows occur swiftly and in lower-viscosity fluids, such as air.

2.5.5. Natural and Forced Flow

Forced convection or forced fluid flow takes place when a fluid is pushed to flow within or throughout a conduit by a pump or a fan, as shown in Figure 2.4a. The up-thrust force impact, on the contrary, is a reaction to the natural convection (thermosiphon effect) of fluid current, in which lighter fluid (warmer fluid) rises and denser fluid (colder fluid) sinks. Figure 2.4b illustrates this fluid action.

2.5.6. Steady and Unsteady Fluid Flow

The kind of fluid flow noted as steady flow is one in which the fluid parameters (including pressure, velocity, and so on) at a particular place do not change during the flow's duration. Unsteady flow is a kind of fluid flow in which the fluid parameters (such as pressure, velocity, and so on) change over time at a particular place. Unsteady flow may be distinguished from steady flow by its lack of a steady state.

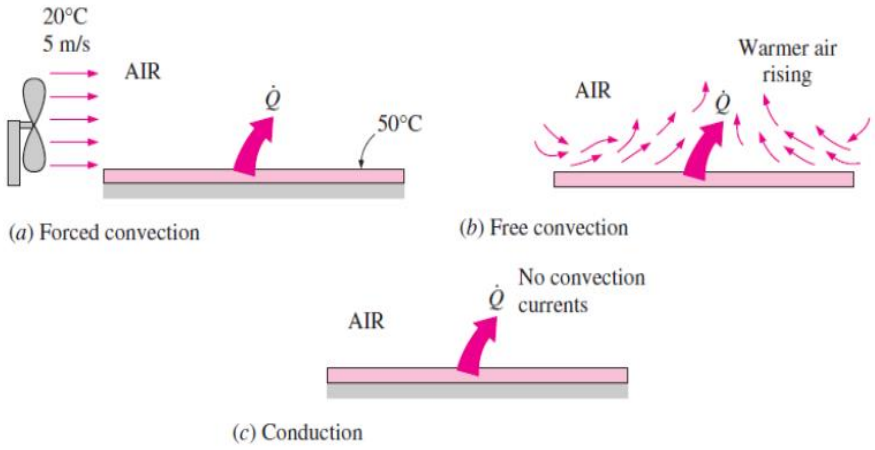

Figure 2.4. Physical mechanism of heat transfer from hot surface to cool surrounding air by convection and conduction [24].

2.6. CONCEPT OF BOUNDARY LAYERS

Knowing the convective heat exchange between a surface solid and a fluid moving over it necessitates an understanding of boundary layers. Velocity and thermal boundary layers are covered in this section.

2.6.1. Velocity Boundary Layer (δu)

Figure 2.5 shows the velocity boundary layer of a flat plate fluid. The y-axis shows normal flow far from the plate surface, while the x-axis shows fluid flow across a flat plate from its leading edge. with the plate's leading verge, the fluid travels *x* with a uniform velocity (v). The fluid may consist of multiple nearby layers piled on top of one another. The no-slip scenario prevents fluid particles in the first layer close to the surface plate from moving. The fluid layer is affected by the friction force between the fluid particles of these two neighboring layers traveling at different speeds at some space from the plate's surface. The velocity approaches $u = 0.99u_\infty$, which is the boundary layer thickness (δu). The velocity boundary layer's flat plate surface has zero fluid flow velocity. The flat plate surface has a superfine laminar sublayer, laminar sublayer, and the buffer layer accompanies turbulent flow. The turbulent layer is third. The free stream region, $u = u_\infty$, is far from the surface [24].

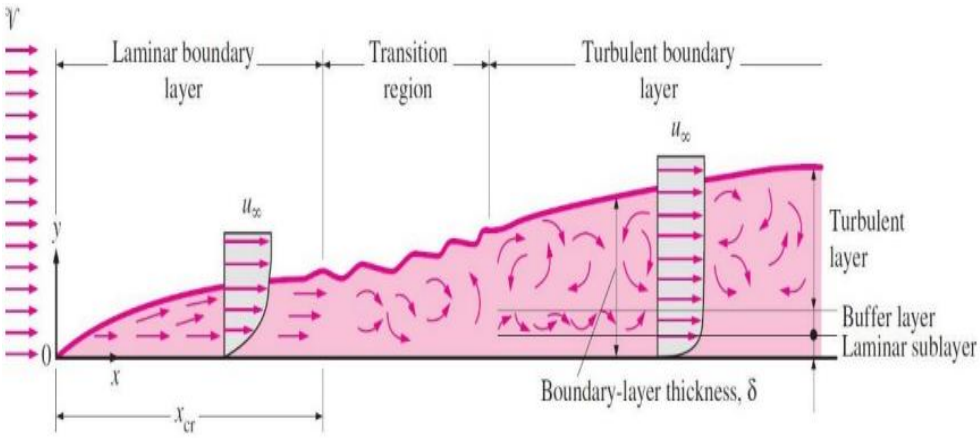

Figure 2.5. Velocity boundary layer development on a flat plate surface [24].

2.7. THERMAL BOUNDARY LAYER (δ_{th})

The thermal boundary layer, like the velocity boundary layer, occurs when there is a temperature difference between the surface plate and the fluid flow. The fluid layer near the heated surface of the plate attains thermal equipoise with it. The energy of the fluid particles are transmitted to those in the subsequent fluid flow layer, and so on. The temperature included in the thermal boundary layer is calculated with the following formula:

$$(T_s - T) = 0.99(T_s - T_\infty) \tag{2.2}$$

Because the effects of heat transmission are go deeper into the fluid flow, the thermal boundary layer thickness rises as the fluid flows away from the leading edge. At any space from the leading edge, using Fourier's equation at the contact between the fluid layer and solid surface plate at y = 0 displays the link between convection and conditions of heat transfer:

$$k_f \frac{dT_f}{dy}\Big|_{y=0} = k_s \frac{dT_s}{dy}\Big|_{y=0} \tag{2.3}$$

where K_f is the thermal conductivity of a fluid and K_s is the thermal conductivity of a solid flat plate [25]. The thermal boundary layer of a cold fluid moving throughout a hot flat plate (T_s) at a steady temperature (T) is seen in Figure 2.6.

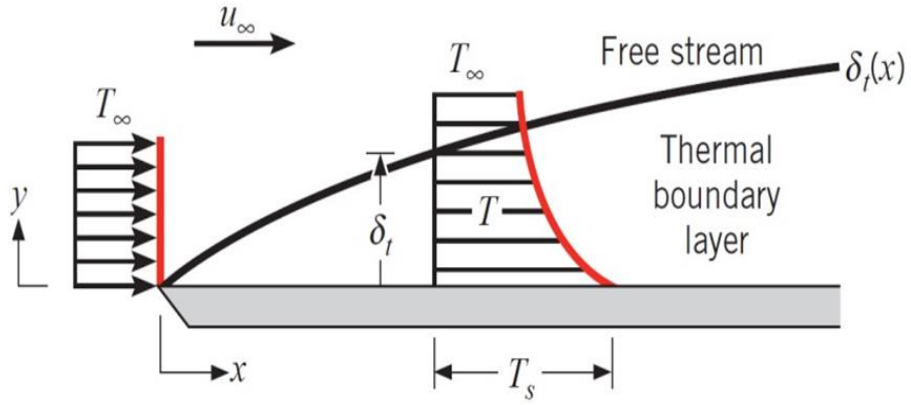

Figure 2.6. Thermal boundary layer development on an isothermal flat plate surface [25].

2.8. BOUNDARY LAYER SEPARATION

Fluid flow around a cylinder should be considered for engineering uses to understand the phenomena of boundary layer segregation, bundles of circular tubes, shell and tube heat transfers, cones, circle PHSs, etc. Figure 2.7 shows the upriver fluid velocity (V) of a cylinder as well as free stream velocity (u_∞) as a function of remoteness (x) from the stagnancy point. The fluid velocity is zero at the stagnancy point. As shown in Figure 2.8, the fluid flow rises because a positive pressure incline ($du/dx > 0$ as $dp/dx = 0$) reaches its extreme at $dp/dx = 0$ and then drops because a negative pressure incline ($du/dx = 0$ as $dp/dx > 0$). The fluid velocity incline at the surface equals zero when the fluid flow slows, and this place is known as the "separation point." The fluid can no longer continue going downstream because its momentum is inadequate to overcome the pressure gradient. The approaching fluid flow also prevents upline flow, and as a result, boundary layer separation becomes necessary. This is the primary cause for the boundary layer to detach from the surface and produce inverse flow and vortices just downstream of the cylinder [25]. The velocity profile of the cylinders. connected with the pressure gradient and separation [25].

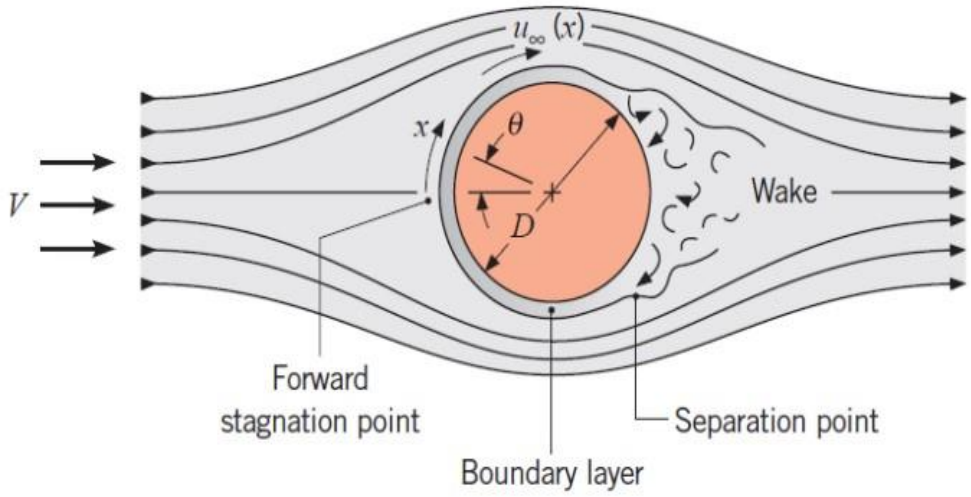

Figure 2.7. Boundary layer separation on a cylinder and formation eddies in the downstream region [25].

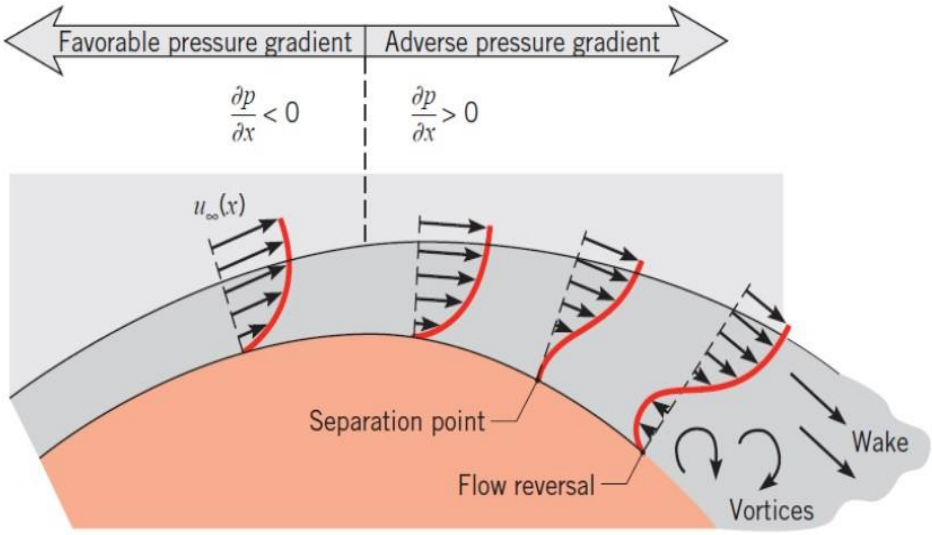

Figure 2.8. Velocity profile associated with pressure gradient and separation on a cylinder [25].

PART 3

LITERATURE REVIEW

3.1. INTRODUCTION

Over the past few decades, with the development of electronic devices and increasing applications in the engineering arena, urging a new philosophy of the heat sink has become a priority in today's world. New solutions must be proficient in dealing with massive heat emissions while maintaining cost and space restrictions. Finned heat sinks are one of the most effective heat management and cooling methods.

Due to the expansion of the use of electronic devices and the hunt for the best ways to cool them over the last decade, researchers are paying attention to the heat sink and how to enhance it. Water, air, and nanofluids are the three most common fluids utilized as heat transfer media in heat sinks. This section presents the research review conducted on the current study.

3.2. EXPERIMENTAL STUDIES

Choudhary *et al.* [26] focused on the experimental examination of heat exchange and the airflow behavior of pin fin heat sinks with and without wings below forced convection. For both in-line and staggered pin fin designs, the fin pitch ratio (*S/D*) and wing size ratio (L_w/D) is changed for the Re range of 6800-15,100. Reducing the *S/D* and L_w/D ratios would enhance friction losses and heat exchange rates. The optimum performance is provided by a pin fin heat sink with wings, an L_w/D ratio of 0.2 and an *S/D* ratio of 2.

In the study by Hatem *et al.* [27], the heat exchange by forced convection in a circular PPFHS was investigated. At a low power of 10 W, the temperature of the

non-perforated fin decreased from 35℃ to 31℃ while the temperature of the perforated fin decreased from 35℃ to 29.8℃. At a maximum power of 250 W, the temperature dropped from 300℃ to 55℃ for the non-perforated fins, and from 300℃ to 38℃ for the perforated fins.

Srikanth *et al.* [28] used four equal-area heaters to investigate the phase change material-based (PCMB) composite 72-pin fin heat sink under individual heat loading. After investigation, the heat inputs were modified across numerous targets while maintaining heater power. Metal heat sinks n-eicosanoid PCM were the first house-based power combinations to be tested. Hotspots caused by spatially non-uniform heat flow would affect the solidification cycle, melting, and heat sink performance. Due to heat sink performance diversity, the researchers utilized the non-dominated sorting genetic algorithm (NSGA-II) to do a multi-objective optimization to find the best discrete power levels that shorten the discharging period and lengthen the charging period.

3.3. NUMERICAL STUDIES

Bakhti *et al.* [29] focused on a numerical study of the jumbled convection of nanofluids in heat sinks with pierced circular fins. Four distinct nanofluids utilized as cooling fluids were TiO_2, Al_2O_3, and Cu sparsed in pure water as the base fluid. The volumetric concentration of nanofluids that were selected fell within the ranges of 2% to 10%. The Re was reduced to 100-400 in order to retain the laminar system and a Richardson number of 1 Ri 22 so as to see how well the heat sink would cool because of the dispersion of nanoparticles in the base fluid. The results showed a considerable optimization in heat exchange in the heat sink as compared to that of pure water. Heat exchange could be improved further by raising the Re and reducing the nanoparticle volume fraction.

Al-Sallami *et al.* [30] used a contemporaneous heat exchange model that was utilized to explore the benefits of utilizing SFHSs, whose cross-sectional aspect ratio was found to be between that of plate fins and pin fins. According to the data, strip fins are an more efficient technique to promote heat transmission, especially when

staggered. Perforating the strip fins improves heat conduction, would reduce pressure loss and heat sink bulk. The relevance of perforated SFHSs in producing 20 lower processor temperatures for decreased power of mechanical consumption for practical 19 applications in microelectronics cooling were also demonstrated.

Al-Damook *et al.* [23] investigated the advantages of PHSs with rectangular slotted, single, and notched pin holes utilizing a conjugate heat exchange model. The results showed that as the size of the rectangular holes increases, the heat transmission rises monotonously while the pressure drop reduces monotonously. Heat transmission and pressure drop measurements with PHSs with numerous circular perforations would reveal favorable features.

Gupta *et al.* [31] investigated the low Re thermal boundary conditions for air as the working fluid, as well as the hydrodynamic and thermal characteristics of a punctured MPF heat sink with varied punctured forms and counts. The results showed that punctured MPFs have higher Nu values and lower ΔP levels than solid MPFs. The studies demonstrated that punctured MPFs are more effective than solid, square-shaped MPFs. Furthermore, punctured MPFs would outperform solid MPFs (by roughly 45%). This study also revealed that, regardless of the number of punctured MPFs, circular-shaped punctured MPFs, would outperform elliptical and square shaped punctured MPFs (η). The performance of the circular shaped punctured MPFs would rise by 30% from one to two punctured MPFs by up to 28% from two to three holes. According to the findings of this study, a solid square MPF heat sink with circular holes offers a greater potential for enhancing thermal management in electronic equipment.

Sahel *et al.* [32] investigated the best HSPF layout and hydrothermal functioning of a heat sink with hemispherical pin fins (HSPFs) in fully turbulent flow. The numerical method used in this work was tested using a heat sink with staggered CPFs. Solid-HSP hydrothermal functioning was quantified and compared to a reference sample. The highest HTPF was 1.87, with a d/H ratio of 0.833 and Re of 21,367. In the final phase, the punctured method was used to optimize the hydrothermal functioning of the basic case. Hydrothermal performance was examined for six punctured designs

with different hole counts. The pattern with the most holes was found to have an HTPF of 1.98, 5.6 times the basic case. The HSPF design also decreased heat sink volume by 76% relative to the reference scenario.

Maji *et al.* [33] Examined the functioning of heat sinks for pierced pin fins of various forms, such as round, elliptical, and diamond shaped forms. Three-dimensional CFD models were created to explore the impact of fin shape, puncture geometry, and puncture size on system function. Heat transmission was also increased by installing square and elliptical staggered pin fins along the flow route at various angles. Multi-Objective improvement under Ratio Analysis was used to select the ideal heat sink configuration. Entropy generations, exergy efficiencies, and irreversibility were estimated for each fin shape with different-sized holes. It was discovered that, up to a point, perforated fins would always dissipate heat faster than solid fins, and that this rate rises considerably as hole geometry and fin shapes change.

Ghyadh *et al.* [34] used a three-dimensional, non-isothermal CFD model to examine the thermal functioning of a heat sink with punctured fins. Four-pin fin heat sink examples with diverse geometrical designs were used and governing equations were discretized utilizing the FVM approach, after which they were solved, and validated using the available experimental data with the multi-physics COMSOL software version 5.3. The experimental and CFD results agreed, proving the validity of the CFD simulation model utilized in this study. According to the findings, the pierced pin fins boost thermal transmission and accelerate heat dissipation. The positioning of the fins was also studied, and the results showed that the layout considerably improved heat transmission. Perforated fins had exhibited higher average heat transfer coefficients than solid fins, and sample 3 had more heat dissipation than the other samples.

Mandal *et al.* [35] conducted a detailed CFD simulation to examine the efficacy of a horizontal heat sink with a vertical punctured pin-fin array. Pin fins were inserted in a staggered pattern onto the base plate of a horizontal sink. This research aimed to observe how the direction angle (β) impacts the efficiency of a heat sink. The angle would range from 0° to 360° by rotating the horizontal sink along a vertical axis that

passed over its center. Data were collected across a wide domain of inflow Re to study the potential of obtaining a perfect orientation angle (β) for optimal thermal functioning. It was found that solid fins of the same dimension would yield the same results. A maximum Nu was reported for perforated fin arrays at an angle of 180°, whereas the optimal angle for solid fins was found to be approximately 120°.

Alfellag *et al.* [36] investigated the impact of an inclined slotted plate-fin mini-channel heat sink with triangular pins on laminar convection heat exchange and fluid flow utilizing a conjugate heat exchange computer model. The shape of the slots and pins were parametrically analyzed to increase the hydro-thermal performance of the heat sink. During the examination, the height of the oblique slot, its angle, and the positioning of the pin near the slot's leading brim were all altered. The Re was between (100-1600). CFD results showed that, compared to the simple mini-heat sink, the total height slot with a 55-degree inclination angle increased the Nu and the hydrothermal functioning factor by up to 1.5 and 1.43, respectively. Furthermore, the Nu and JF factor of the heat sink were 1.84 and 1.54 times higher, respectively, than the straight channel.

Haque *et al.* [37] carried out a numerical examination to analyze the effect of forced convection heat exchange for a range of inventive-shaped pin fin heat sink styling by modifying the influence of different parameters on the fluid and solid fields. The paper shows one conceivable configuration for such a heat sink design, which employs cutting-edge pin fins in the Twisted and Grooved form. Various hole types and alignments would enhance the surface area, increasing the heat exchange amount and HTP. The RANS k turbulence model and Navier-Stokes equations were used in the study's modeling.

Ahmadian-Elmi *et al.* [38] investigated the pin-fin heat sink, one of the most prevalent cooling systems, and computationally modeled them using the finite volume approach, and improved all geometric elements affecting functioning based on thermal and hydraulic functioning (FOM). Fin height, diameter, number, and transverse pitch were the geometrical features with which they worked. It was found that by adjusting these values steadily would increase pin-fin heat sink performance,

and that pin-fins should be tapered. Changing the fin shape affected h and ΔP, thereby improving system functioning. The optimization phase enhanced pin-fin heat sink performance by almost 17%.

3.4. EXPERIMENTAL AND NUMERICAL STUDIES

By utilizing computational fluid dynamics (CFD), we can validate the benefits of utilizing punctured pin fin heat sinks. Holes on heat sink pins were created and constructed to evaluate their influence on heat transmission and pressure. The results indicated that as the number of pin holes grew, so did the Nusselt number. Pinhole positions, on the other hand, have less of an influence, according to Al-Damook *et al.* [6].

The ideal design of a PPFHS-PS was created in this study utilizing CFD-ACE+ and the LMM to obtain the peak thermal functioning factor under a defined fin volume limitation. In the current study, which investigates the execution of punctures and splitters on a pin fin, the diameter of the pin after it has been punctured, the diameter of the pin, and the length of the splitter are taken into account as design parameters. The hydrothermal functioning of a PPFHS, a PPFHS-P, and a PPFHS-S were examined. The PPFHS-PS were shown to increase the thermal functioning factor greatly. The numerical design scenarios show that the percentage optimization for the PPFHS-P, PPFHS-S, and PPFHS-PS were 4.9%, 5.2%, and 10.1% greater than the original PPFHS with an entry velocity of 5.0 m/s. This demonstrates that if punctures and splitters are employed in the PPFHS-PS design at the same time, the single contributions of thermal functioning factor enhancement of the PPFHS-P and PPFHS-S may be contributed by Huang *et al.* [39].

In the study by Khattak *et al.* [40], critical reviews were made of numerous heat sink designs, evaluating the limits, use, and future advancements in the creative heat sink. This research began with a concise and detailed description of the importance of heat sinks, their methodology, their application to contemporary heat loss problems, statistical data on a variety of heat sink designs, and a full assessment of previous work.

Baldry *et al.* [41] in their study built and experimentally verified a computational model for building high-functioning, small-scale heat sinks for use with a thermoelectric cooling cap. As a compromise between minimizing burn injuries and decreasing the quantity of heat that was needed for dispersal, the anticipated average base temperature was established at 45℃. The design hampered the load of the heat at 2.15 W. Numerous computational iterations were used to develop a perfect natural convection heat sink with a calculated thermal resistance of 10.9 kW and a base temperature of 44.4℃. This styling, which contained an internal cavity in a tapered pin array, was able to achieve a steady state base temperature that was 11.7℃ lower than a standard styling with a 51% lower surface area and far less material.

The advantages of multiple holes and slots in a PFHS utilizing a conjugate heat exchange for further experiments and models were examined Tariq *et al.* [42]. The heat exchange and ΔP of two unique PFHSs with punctures and slots were investigated. The experimental results of the air-cooled heat sink validated the conjugate heat exchange CFD model, the results of which would show that new PFHSs have a greater heat transfer coefficient than plane fins without slots and holes. Furthermore, the novel plate-fin heat sinks was shown to demand less fan power since they had a lower ΔP than the conventional PFHS. For a Re range of 13,049 to 52,195, the Nu of the novel PFHS 1 and 2 were found to be 42.8% and 35.9% higher, respectively, than those of the planar PFHS. It was also found that slots and holes provide value by lowering the volume of the heat sink.

Song *et al.* [43] examined heat dissipation from a heat sink with punctured fins on a cylindrical base. The size and number of holes per fin were examined to improve heat sink heat dissipation. A greater number of very small holes improved heat dissipation. However, threshold values for perforation size and the number decreased heat resistance. The Rayleigh number, fin count, fin inclination angle, and heat sink direction angle quantified heat-dissipation performance. The numerical analytical approach was experimentally verified. As the number of fins increased, the heat-dissipation of the surface of the heat sink increased proportionally, lowering thermal resistance. The fin inclination angle affected thermal resistance, allowing the orientation angle to be changed to maintain heat-dissipation functioning. The thermal

resistance of the cylindrical heat sink with pierced fins was predicted using this correlation. The estimated correlation predicted thermal resistance to be within 5.25 percent.

Towsyfyan *et al.* [44] used PFHSs with symmetrical half-round hollow pins that were vertically organized and subordinated to parallel flow and built using good thermal design. CFD research was used to examine the thermal performance of the many possible designs using different hollow pin interior and exterior diameters. Based on these few data points, a feed-forward back-propagation neural network forecast the base temperature and pressure drop to predict the optimal form of the hollow pins. The reference data and neural network simulations were within 1.24%. CFD was then used to determine the best heat sink design by examining how pin pitch affects thermal performance. The ideal inner and outer pin and fin radii were found to be 1.08 mm, 1.2516 mm and 3.6 mm. Correlation equations would also predict 88.98% and 88.81% of Ff and Nu.

Abuşka *et al.* [45], in their research, tested CPFHSst and CPFHSmst conical PFHSs for thermo-hydraulic performance by comparing a flat heat sink and heat sink with traverse-cut pin-fins that were parallel to and perpendicular to the airflow. The adjusted staggered fin placement was 2-7℃ less than the staggered surface and junction temperatures as heat sink fin location affected parameters with increasing Re. The Rth of the adjusted model was 5.3%, 5.8%, and 3.5% lower than the staggered model despite the greatest P of CCPFHSperp at 6.7 Pa, 6.9 Pa, and 7.4 Pa. The updated model had a 6.4% advantage over CCPFHSperp and a 17.4% advantage through the staggered model for the test powers. The reformed model outperformed CCPFHSperp by 13.3%, 12%, and 10.9%, respectively.

In this study, the cooling process using a modern design of a perforated conical PHS was tested on the functioning of the heat sink while utilizing air as the heat exchange medium. The results of this study were examined. It is important to be aware of the influence that the number of holes and the inclination angle of the conical pin, as well as the ΔP and the Tb, have on the Nu.

PART 4

NUMERICAL SIMULATION

4.1. INTRODUCTION

With the increasing speed of computers and the high cost of physical experiments, computational fluid dynamics (CFD) has been increasingly utilized for the heat transfer and fluid flow modeling of finned channels as a heat sink. CFD enables the user to obtain many designs in record time and with high efficiency and predict the results before conducting physical experiments. The reason for the increasing use of this software is the use of commercial symbols to model different cases in engineering applications by making them more attractive and effective. The mathematical formula for the CFD includes a set of partial differential equations (*PDE*) which are solved numerically using the Finite Volume Method (*FVM*). In this study, the governing equations were solved using ANSYS-Fluent v.20_R2. To ensure the accuracy of the results, a set of CFD simulation validations were performed prior to the current simulations of the study.

4.2. RESEARCH METHODOLOGY

The methodology of this study covers CFD simulation using ANSYS-Fluent v.20_R2. The shape was designed using the Solid Works program, and by using ANSYS-Fluent, the solution would include the determination of the solid part (heat sink) and the fluid part (test channel), defining the boundary conditions, determining the fluid properties, executing the solution, and displaying the results. A set of different tests were performed prior to simulating the current study in order to validate the results. Selecting the type of mesh and the density of the mesh, many meshes were checked for a suitable mesh system referred to as the “grid independence test” (GIT). Dense mesh takes a long time to simulate, and low-density

mesh results are inaccurate; therefore, GIT would determine the required density of the mesh and save simulation time to obtain accurate results so as to ensure the validity of the results of this work compared with the results in the literature through numerical and experimental data. The results would be considered acceptable if the error rate does not exceed 5%. CFD simulation work is often represented by the scheme shown in Figure 4.1.

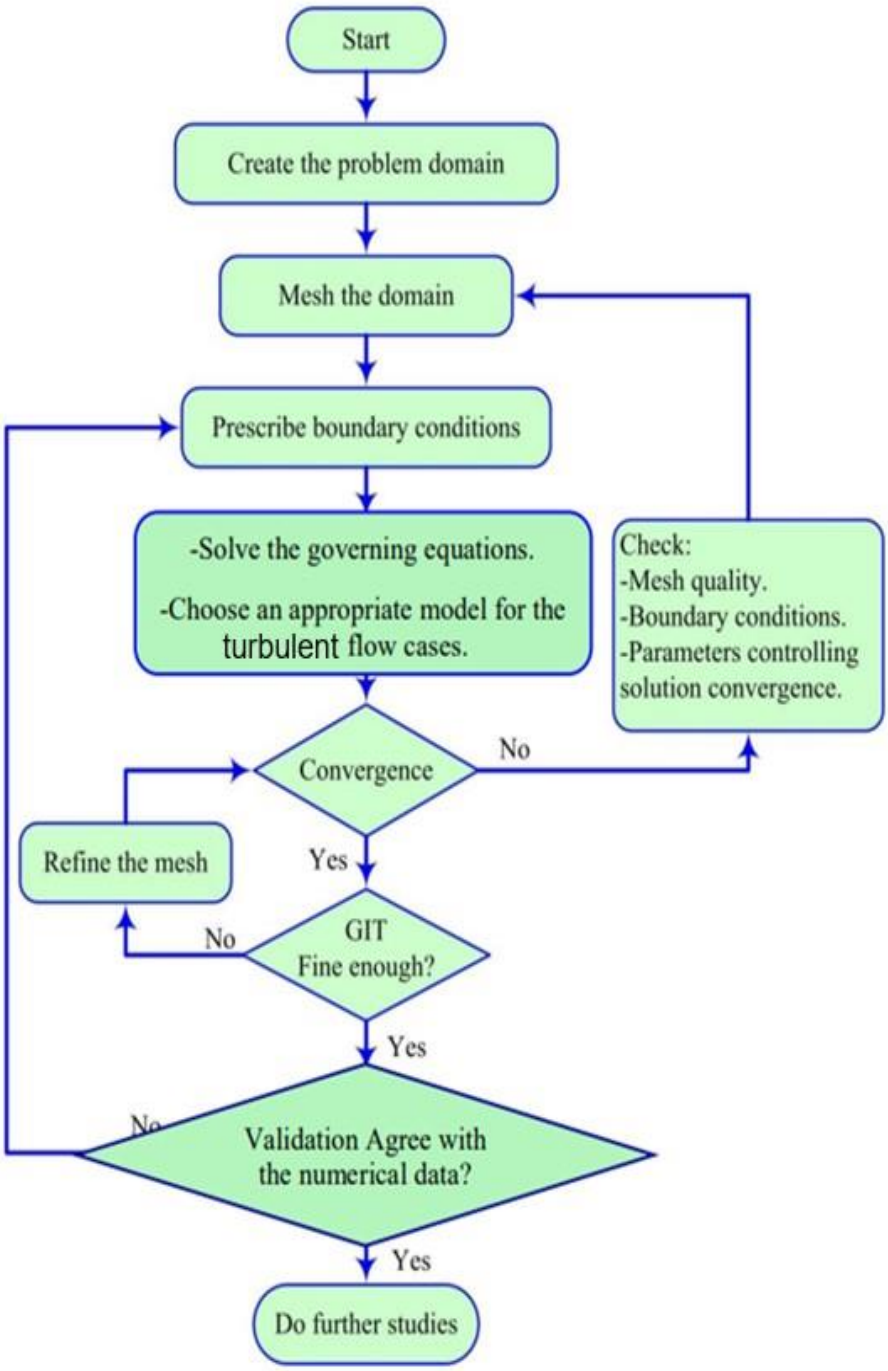

Figure 4.1. Numerical simulation flow chart.

4.3. PHYSICAL MODEL AND ASSUMPTIONS

The schematic diagram of the design studied in this research is shown in Figure 4.2. The base area of the heat sink is 50 mm × 50 mm × 2 mm i.e., width (Wb) × length (Lb) × height (Hb), respectively. Pin diameter (Df) and pin height (Hf) are 2 mm and 10 mm, respectively, and the number of pins (Nf) is 64 pins, arranged in eight rows following the in-line array method, with the distance between each pin (S) being 6.25 mm. This research studies four shapes of conical pins according to the inclination angles of the cone (Φ). These inclination angles of the cone used Model A = 1°, Model B = 2°, Model C = 3°, Model D = 4° and S = 0°, as shown in Figure 4.3. The conical pins are made into four shapes for each cone. For example, Model A is studied in four cases of inclination angles of conical pins (Φ): the first case (A0) means that the cone is without holes, the second (A1) means the cone contains one hole, the third (A2) means the cone contains two holes, and A3 means the cone contains three holes with each hole diameter (Θ) being 1 mm. Model S is a standard model without perforations or tilt angle (i.e., Φ = 0). The dimensions of the test channel are Wc = 6.5 mm, Lc = 100 mm and Hc = 10 mm, as shown in Figure 4.4. The thermophysical properties of air and aluminium are listed in Table 4.1 [24]. The degree of inclination of the cone (Φ) is calculated using $\tan(\Phi) = (r_1 - r_2)/h_F$ such that r_1 and r_2 are the base radius and head radius, respectively.

Table 4.1. Thermophysical properties of air and aluminum at a temperature of 18℃.

Thermal properties	**Air**	**Aluminum**
ρ **(kg/m^3)**	1.2124	2712
***Cp* (J/kg K)**	1007	871
***k* (W/m K)**	0.02498	202
μ **(kg/m s)**	1.8158E−05	----

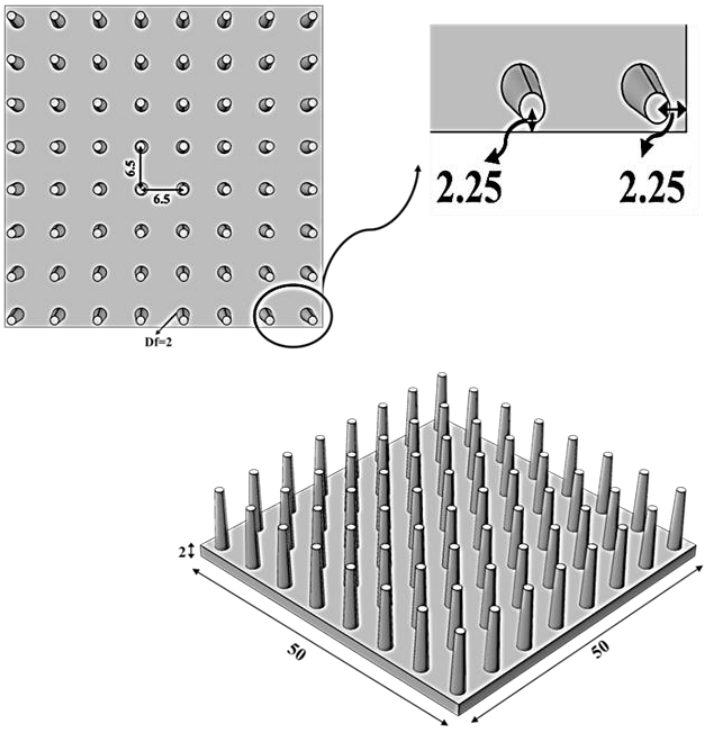

Figure 4.2. Heat sink dimensions in mm.

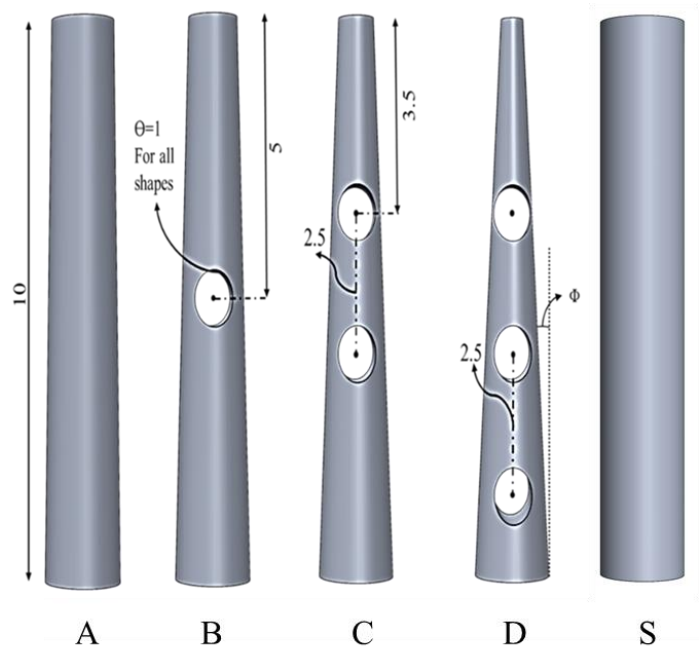

Figure 4.3. Design of fin shapes in the current study (A = 1°, B = 2°, C = 3°, D = 4°, S = 0°) in mm

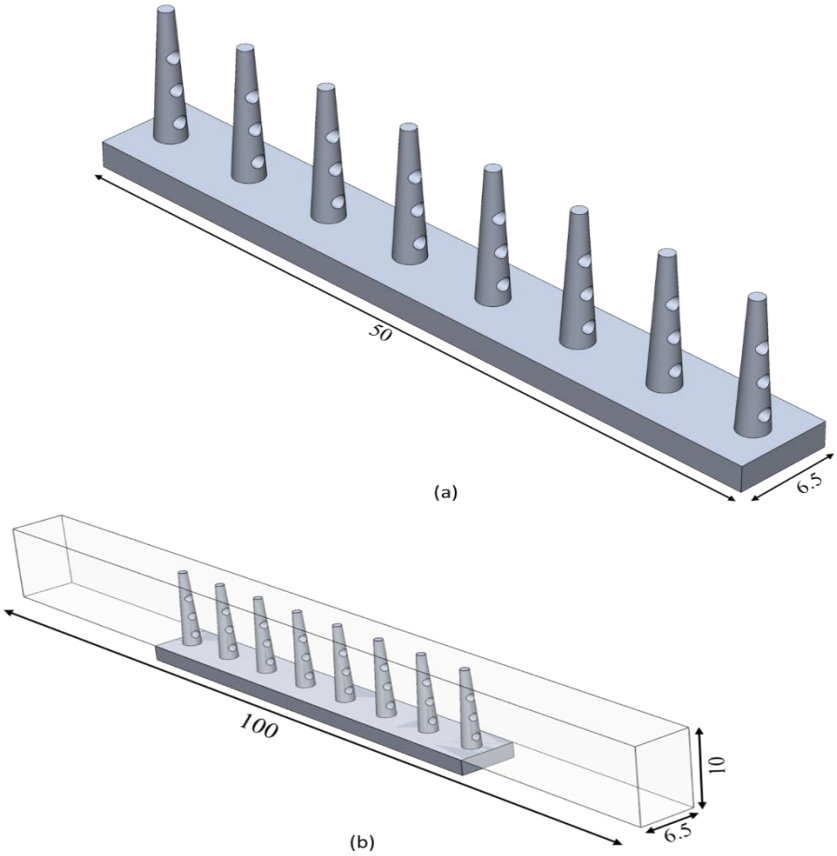

Figure 4.4. (a) Dimensions of the heat sink slice in mm; (b) Dimensions of the test channel in mm.

4.4. GOVERNING EQUATIONS FOR TURBULENT AIRFLOW MODEL

Several previous publications, namely [23], [30] and [46], have successfully employed the Reynolds-Averaged Navier-Stokes (RANS) equations to simulate turbulent flow in heat sinks. By averaging the terms of the RANS equations over time, RANS models can account for turbulence fluctuations by dividing the velocity into a middle value plus variation. Therefore, this technique is the most extensively used and which can be used to solve turbulent flow problems in CFD approaches. By decomposing variables into mean and fluctuation components using Equation 4.7 (continuity), Equation 4.8 (momentum), Equation 4.9 (energy), Equation 4.10 (conjugate heat transfer), and Equation 4.11, we derive the RANS equations, as follows:

$$\nabla \cdot \rho \underline{U} = 0 \tag{4.7}$$

$$\nabla \cdot (\rho \underline{U})\underline{U} = \nabla \cdot \left(\underline{\underline{\sigma}} - \rho \overline{\underline{U}}' \overline{\underline{U}}'\right) \quad (4.8)$$

Where

$$\underline{\underline{\sigma}} = -p\underline{\underline{I}} + \mu\left(\nabla \underline{U} + [\nabla \underline{U}]^T\right) \text{ and } -\rho \overline{\underline{U}}' \overline{\underline{U}}' = \mu_t\left(\nabla \underline{U} + [\nabla \underline{U}]^T\right) - 2/3(\rho k \underline{\underline{I}}) \quad (4.9)$$

Here, μ = air viscosity (), ρ = density (), $\underline{U}$ and $\overline{U}'$ respectively are the average and turbulent fluctuation velocity vectors, P = pressure, k = turbulent kinetic energy, and $\underline{\underline{I}}$ is the unit tensor, all of which described by Equation 3, which also represents the Newtonian and Re stress tensors, respectively. As can be seen in Figure 4.5, the RANS equations for the temperature domain (T) with a power supply of $\dot{Q}$ watts are solved by applying the energy equation in the solid and fluid domains, which are referred to as coupled boundary conditions as a model conjugate heat transfer, using the following equations:

$$\rho \underline{U} \cdot \nabla\left(C_p T_f\right) = \nabla\left(k + \frac{C_p \mu_t}{\mathrm{Pr}_t}\right)\nabla T_f + \dot{Q} \text{ (For the fluid domain)} \quad (4.10)$$

$$\nabla(k_s \nabla T_s) = 0 \text{ (For the solid domain)} \quad (4.11)$$

where Cp is the specific heat capacity of air, t the turbulent eddy viscosity, Pr_t the turbulent Prandtl number, U the velocity of the air, T_f the fluid temperature, T_s the solid temperature, k_f the thermal conductivity of the fluid, and k_s the solid thermal conductivity [47].

The SST model equations are:

$$\nabla \cdot (\rho k \underline{U}) = \tilde{P}_k - \beta^* \rho k \omega + \nabla \cdot [(\mu + \sigma_k \mu_t)\nabla k] \quad (4.12)$$

$$\nabla \cdot \left(\rho \omega \underline{U}\right) = \alpha \rho S^2 - \beta \rho \omega^2 + \nabla \cdot [(\mu + \sigma_\omega \mu_t)\nabla \omega] + 2(1 - F_1)\rho \sigma_{\omega_2} \frac{1}{\omega} \nabla k . \nabla \omega \quad (4.13)$$

where F_1 is defined as the blending function thus:

$$F_1 = \tanh\left(\left\{min\left[max\left(\frac{\sqrt{k}}{\beta^* \omega y}, \frac{500v}{y^2 \omega}\right), \frac{4\rho\sigma_{\omega_2} k}{CD_{k\omega} y^2}\right]\right\}^4\right) \tag{4.14}$$

$$CD_{k\omega} = max\left(2\rho\sigma_{\omega_2}\frac{1}{\omega}\nabla k \cdot \nabla\omega, 10^{-10}\right) \tag{4.15}$$

The turbulent eddy viscosity is calculated as follows:

$$v_t = \frac{a_1 k}{max(a_1\omega, SF_2)} \tag{4.16}$$

where F_2 is a second merging function and S is any invariant strain rate measure defined by:

$$F_2 = \tanh\left(\left[max\left\{2\frac{\sqrt{k}}{\beta^* \omega y}, \frac{500v}{y^2 \omega}\right\}\right]^2\right) \tag{4.17}$$

The SST model employs a production limiter to control the growth of turbulence in standstill zones.

$$P_k = \mu_t \frac{\partial u_i}{\partial x_j}\left(\frac{\partial u_i}{\partial x_j} + \frac{\partial u_j}{\partial x_i}\right) \rightarrow \tilde{P}_k = min(P_k, 10\beta^* \rho k\omega) \tag{4.18}$$

The empirical constants for the turbulent model are [48]:

$$\beta^* = 0.09$$
$$\alpha_1 = \frac{5}{9}$$
$$\beta_1 = \frac{3}{40}$$
$$\sigma_{k1} = 0.85$$
$$\sigma_{\omega_1} = 0.5$$
$$\alpha_2 = 0.44$$
$$\sigma_{k2} = 1$$
$$\sigma_{\omega 2} = 0.856$$

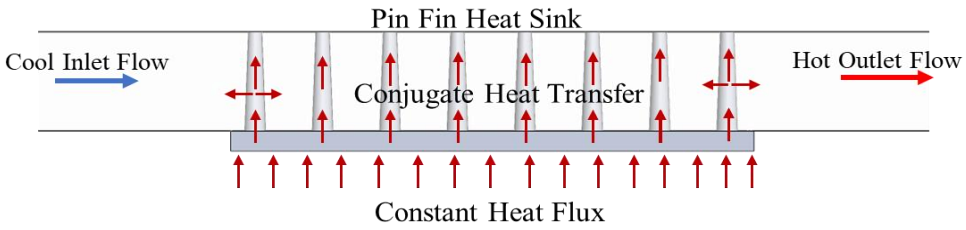

Figure 4.5. Conjugate heat transfer model of pin fin heat sink.

4.5. BOUNDARY CONDITIONS

Problems involving heat transfer and fluid flow require appropriate boundary conditions (*BCs*). As a result, *BCs* for the current problem in this study are presumptive, as indicated in Table 4.2 and Figure 4.6.

4.5.1. On the Pins

Through linked BCs at the solid/fluid interface, the rejected heat conduction rate via the heat sink made of aluminum pins is equiponderant with the obtained heat transfer convection into the moving fluid stream. That is, each pin fin has two BCs: a fluid surface that symbolizes airflow and a solid surface that serves as the pin fin heat sink's material and is used for conjugate heat transfer.

4.5.2. At the Bottom Wall of the Heat Sink

A constant heat flux is applied to the bottom wall of the heat sink (Q = 50 W). There is no slip state, so the fluid velocity is zero in each direction, Uy = Ux = Uz = 0.

4.5.3. At the Inlet Side

According to [48], [23] and [30], inlet fluid velocity is adjusted to a sequence of values as U_x = (6.5, 8, 10, 12) m/s and $U_y = U_z = 0$. Additionally, the temperature of the inlet air (T_{in}) remains steady at 18°C. The flow arriving via the inlet air temperature boundary has a turbulence intensity set at 5% [48]. Most industrial electronic applications use heat sinks with Reynolds numbers ranging from 1,300 to

50,000 [49]. Re is therefore changed from 3,400 to 6,400 in this study as a turbulent airflow to lower the consumption of fan power and noise levels of the fan to acceptable levels, especially in the home or office.

4.5.4. Right and Left Sides

According to [30], uniform fluid flow and symmetry in the fin arrays produce a symmetric boundary condition on the left and right sides of the channel. Therefore, to reduce the model field and number of nodes, computations are only performed on the eight pin fin, not the entire array of pin fins. This saves computer memory and shortens the time for a convergent solution.

4.5.5. Other Surface Walls

No heat transfer occurs through any other walls or surfaces in the computation field since they are all supposed to be adiabatic surfaces with zero heat flux. Due to the rigidity of the walls, which results in zero air velocity in all orientations, a no-slip condition is used [23]; therefore, Ux = Uy = Uz = 0 is set.

Table 4.2. Boundary conditions of the conjugate heat transfer model.

Locations	**Fluid Conditions**	**Thermal Conditions**	**Locations**	**Fluid Conditions**	**Thermal Conditions**
Inlet	U = (6.5-12) m/s	T = 18℃	**Bottom wall of heat sink**	U = 0 m/s	$\dot{Q}$ = 50 W
Right and left sides (symmetry)	$du/dy = 0$	$dT/dy = 0$	**Outlet**	P_{gage} = 0 Pa	$dT/dx = 0$
Top wall and other walls	U = 0 m/s	$dT/dz = 0$	**Pin heat sink**	U = 0 m/s	$k_{\text{air}} \cdot \frac{dT_{\text{air}}}{dn} = k_S \cdot \frac{dT_S}{dn}$

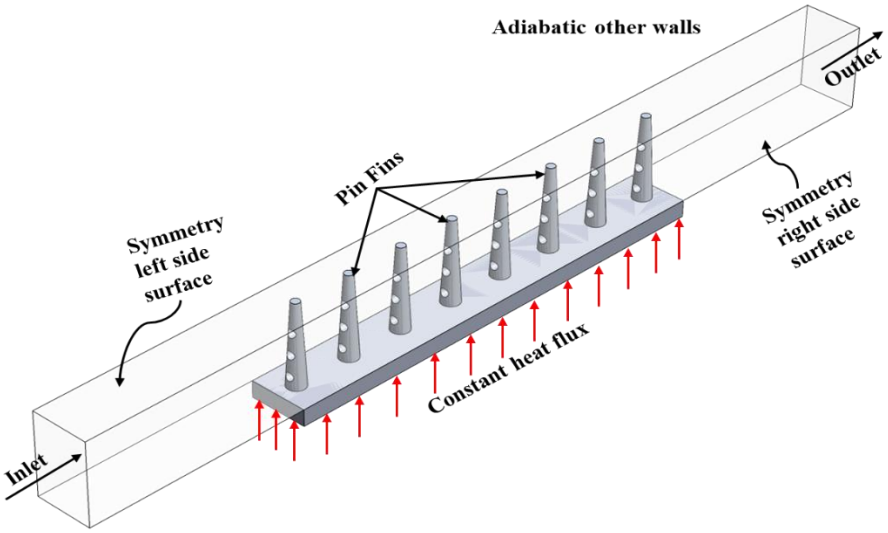

Figure 4.6. Schematic diagram of the flow domain used in the CFD analyses, showing eight perforated pin fins.

4.6. GRID INDEPENDENT TEST

The grid generation assessment of the simulation is one of the most crucial test of the CFD simulation. The physical domain is completely covered by the grid, a very small grid geometric structure. Grids are used to calculate individual sizes to apply conservation laws. The first step was computing the numerical solution equations describing the physical grid formation process. The success of the solution depends on the quality of the mesh. A good mesh can be created by improving the quality of the solution; however, utilizing a grid that is not properly developed causes deviations from the numerical solution. The Hexahedron, Tetrahedron, Quadrilateral Pyramid, and Triangular Prism are three-dimensional grid building blocks. A sample of different sizes (grid density) is tested to obtain the appropriate mesh density, as shown in Table 4.3. In the case of solid conical pins, we use the 964023 element, and in the case of perforated conical pins, we would use the 1106539 element.

Table 4.3. Effect of the amount of Grid Elements on the Collected Data.

Model	Nodes	Element	Temperature (℃)	Error	Pressure drop (Pa)	Error
Solid conical pin heat sink Model C0	24981	123003	112.00	11.99%	25.13	1.11%
	56441	289240	98.57	7.43%	24.85	2.13%
	178787	**964023**	**91.25**	**0.055%**	**24.32**	**0.164%**
	416567	2287333	91.30	------	24.28	------
Perforated conical pin heat sink Model C3	26900	131136	102.21	8.06%	23.53	4.89%
	61280	311798	93.97	9.55%	22.38	2.32%
	296551	**1106539**	**85.00**	**0.035%**	**21.86**	**0.732%**
	524782	2868117	84.97	------	21.70	------

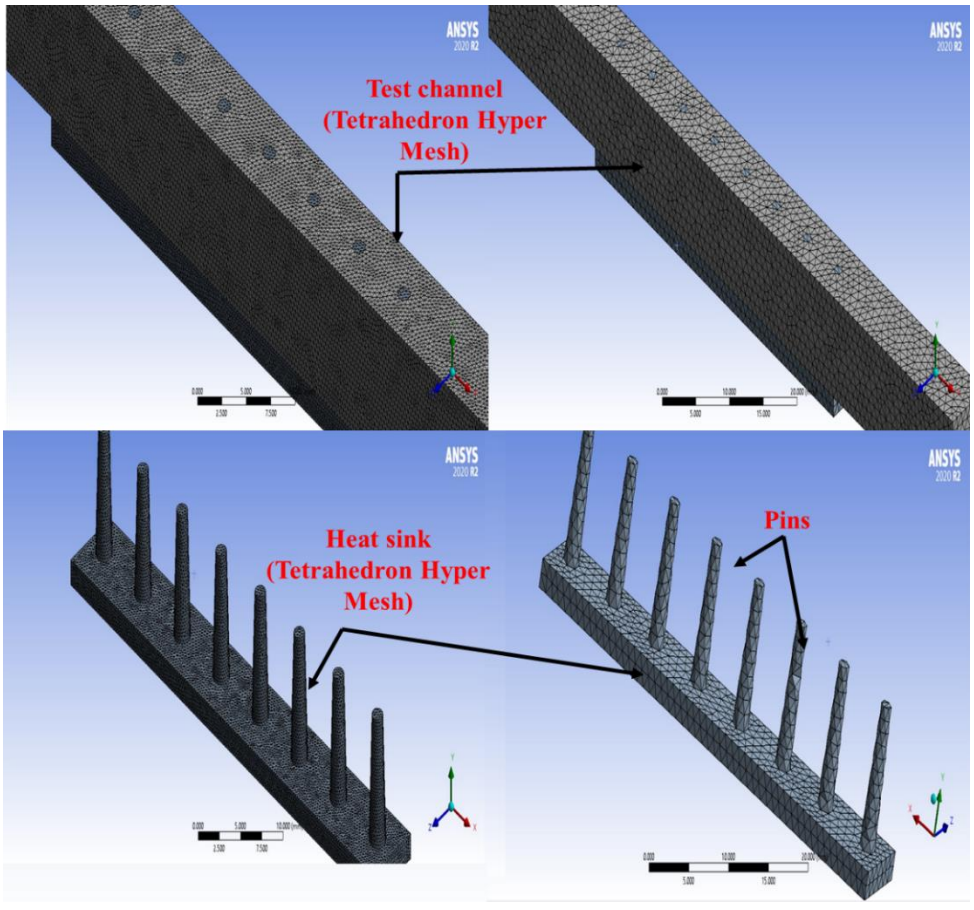

Figure 4.7. Density of grids used in the grid independence test.

4.7. NUMERICAL PROCEDURE

4.7.1. Numerical Simulation

CFD is currently being utilized to investigate how pin perforations affect heat exchange rises and how pressure drops decrease with the latter directly affecting the power desired to drive cooling air over PPHSs, which is determined by the flow amount and pressure drop output [50]. The ANSYS FLUENT-CFD software is used to numerically inspect and analyze models of the heat sink. This application utilizes the FVM approach to solve the governing equations. FVM solves the RANS equations in three dimensions, coupled with the energy and continuity equations to illustrate the dynamic airflow and heat exchange around the PHSs. The continuity equation is met utilizing the Semi-Implicit Method for Pressure Linked Equations (SIMPLE). The RANS equations and the energy equation are computed using second-order upwind discrimination techniques to decrease numerical errors. Each model comprises three parts: the initial component of the inlet section is a smooth conduit long enough to achieve a completely turbulent flow state. The second domain is a pinned heat sink (test portion) with eight symmetrical aluminum pins that follow the first domain. The last portion is the outlet section, which comes after the test section and is sufficiently long to avoid any boundary condition response in the test section. Every one of the components has the same cross-section (6.5 mm × 10 mm). As air passes across all three of these sites, the Reynolds number ranges fluctuate. In the current numerical study, a great amount of heat sink technology is inspected to discover the optimal model that delivers minimum pressure loss, maximal heat exchange, and a minimum CPU temperature.

4.7.2. Numerical Solution (Processing)

The airflow thermal is simulated as a three-dimensional, steady-state, turbulent airflow, with steady heat flux at the underside of heat sinks and a k-SST model, based on the CFD research of solid pins. This model analyzes airflow, pressure drop, and heat exchange via every heat sink type [30].

4.7.3 Numerical Calculation

The following are estimates of the average *Nu* and the average h_m for convection:

$$Nu = \frac{h_m D_h}{k} \tag{4.19}$$

$$h_m = \frac{Q}{A_p\left[T_W - \left(\frac{T_{\text{out}} + T_{\text{in}}}{2}\right)\right]} \tag{4.20}$$

$$D_h = 4\frac{Ac}{P} = 2\frac{W_C \times H_f}{(H_f + W_c)} \tag{4.21}$$

Equations 4.19-4.21 involve the projected base area of the heat sink (A_p), the top surface temperature of the heat sink (T_w), the thermal conductivity of air (k), the average air temperatures at the inlet (T_{in}) and outlet (T_{out}), and the hydraulic diameter of the channel (D_h).

The Reynolds number (*Re*) is calculated from the following formula:

$$Re = \frac{\rho.U.D_h}{\mu} \tag{4.22}$$

The pressure drop ΔP from the inlet to the outlet of the test section's heat sink is defined as follows:

$$\Delta P = P_{\text{outlet}} - P_{\text{inlet}} \tag{4.23}$$

4.8. VALIDATION WITH PREVIOUS STUDIES

To validate the model's output, the variation of h_p, ΔP, and the heat sink's base temperature T_{base} were compared with the numerical data of Al-Sallami *et al.* [30] to study the convective heat transfer of cylindrical pins numerically. The validations showed excellent agreement with Ref [30] with an error percentage is nearly less than 5%, as shown in Figure 4.8. For this reason, with accurate numerical modeling, heat sink calculations will be performed using the conical pins of the present study.

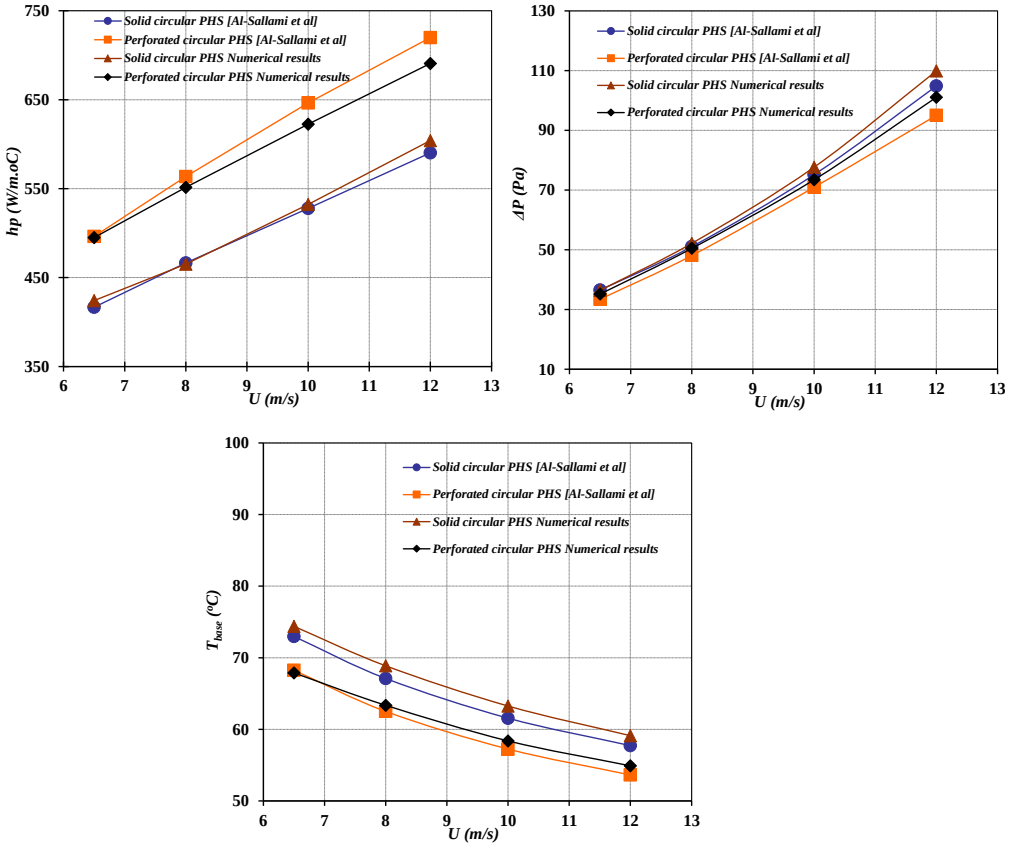

Figure 4.8. Validation for heat transfer coefficient, pressure drops and base temperature

Table 4.4. Validation error rates

Heat Transfer Coefficient					
Solid circular PHS [Al-Sallami et al.]	Solid circular PHS Numerical results	Error rate for solid	Perforated circular PHS [Al-Sallami et al.]	Perforated circular PHS numerical results	Error rate for perforated
416.6320166	424.134	2%	496.2732919	495	0%
466.5280665	465.1855	0%	563.5610766	551.412	2%
527.8586279	532.33	1%	646.3768116	622.556	4%
590.2286902	604.083	2%	719.8757764	690.786	4%
Pressure Drops					
Solid circular PHS [Al-Sallami et al.]	Solid circular PHS Numerical results	Error rate for solid	Perforated circular PHS [Al-Sallami et al.]	Perforated circular PHS Numerical results	Error rate for perforated
36.48	36.4222	0%	33.4765625	35.18726	5%
51.04	52.13427	2%	48.1	50.47518	5%
75.12	77.625	3%	70.9375	73.43018	3%
104.8	109.8618	5%	96	101.0282	5%
Base Temperature					
Solid circular PHS [Al-Sallami et al.]	Solid circular PHS Numerical results	Error rate for solid	Perforated circular PHS [Al-Sallami et al.]	Perforated circular PHS Numerical results	Error rate for perforated
72.97959184	74.38245	2%	68.25462012	67.88306	1%
67.10204082	68.87032	3%	62.50513347	63.35758	1%
61.55102041	63.25657	3%	57.24845996	58.38439	2%
57.71428571	59.11629	2%	53.63449692	54.90573	2%

PART 5

RESULTS AND DISCUSSION

5.1. INTRODUCTION

In this section, the results extracted from the Computational Fluid Dynamics (CFD) program are presented. The results are divided into four cases, as we mentioned earlier, namely A = 1°, B = 2°, C = 3°, D = 4°, each case of which has four forms: solid, one hole, two holes, and three holes, in addition to Model S. A total of 64 cases were studied with velocities ranging from 6.5 m/s to 12 m/s. The Nusselt number, pressure drop, and base temperature of the heat sink were calculated. T_{in} is constant in all cases at 18°C. Q_{flux} = 20,000 W/m^2 was constant.

5.2. COMPARISONS OF NUSSELT NUMBERS FOR DIFFERENT PERFORATION NUMBERS AND CONE INCLINATION ANGLES

The average Nu was compared for four cases of conical pins (pin without hole, pin with one hole, pin with two holes, and pin with three holes). In Figure 5.1, it can be observed that the Nu would be enhanced with the increase in the airflow velocity and the increase in the number of holes for the conical pins due to combining the impact of increasing the production of localized air jets and surface area. The Nusselt number decreases when increasing the angle of inclination of the cone due to the reduction in the material of conical pins. It is also observed that in the two models, C and D, when the number of holes increases to more than two, the Nusselt number gradually decreases. Model A2 achieved the highest improvement rate in the Nusselt number, which was almost 7%, followed by Model B3, with an improvement rate of nearly 4%. Models C and D do not improve the Nusselt number.

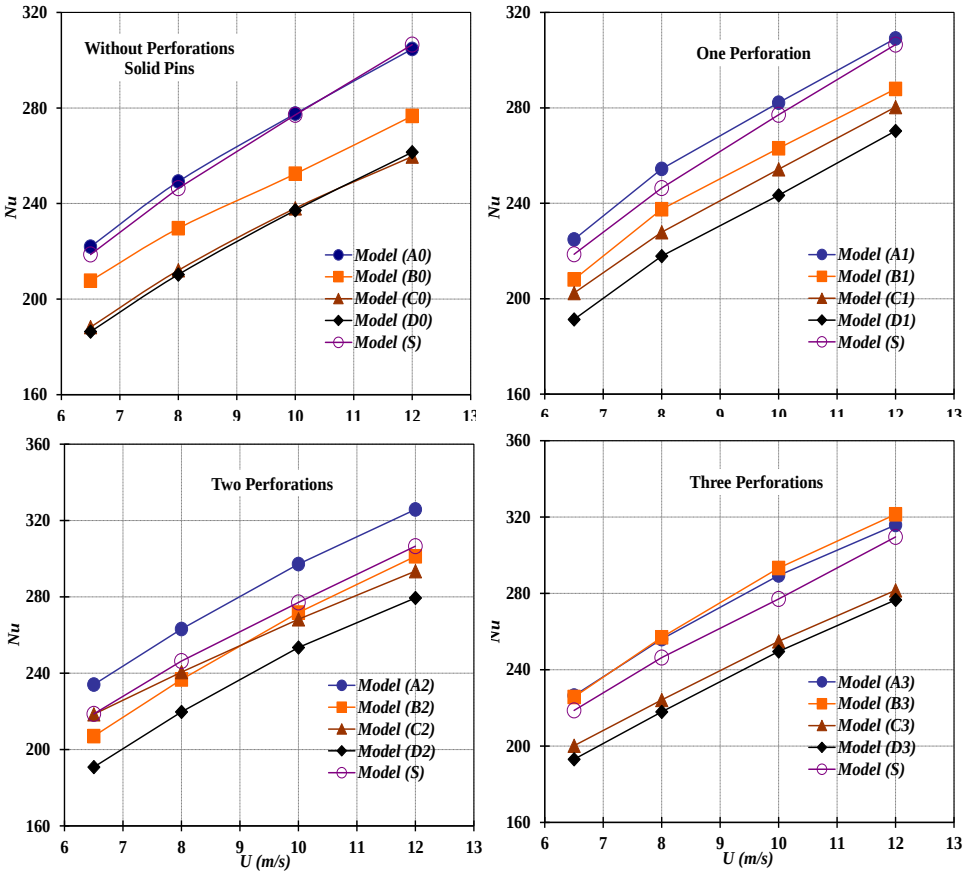

Figure 5.1. Comparisons of Nusselt numbers for different perforation numbers and cone inclination angles.

5.3. COMPARISON OF PRESSURE DROP FOR DIFFERENT PERFORATION NUMBERS AND CONE INCLINATION ANGLES

The pressure drop (ΔP) was compared for four cases of conical pins (pins without perforations, pins with a single perforation, pins with double perforations, and pins with triple perforations) and different cone inclination angles (Φ) (Model A, Model B, Model C, Model D, and Model S). Through the pressure drop charts, we observe that ΔP increases with the increase in the velocity of the airflow inside the test channel. Furthermore, ΔP decreases with the increase in the number of holes for the conical pins and decreases with the increase in the angle of inclination of the cone due to a greater amount of air flowing over these conical pins and perforations. The best performing model for improving pressure drop is Model D3, where the improvement rate was approximately 49%. The lowest improvement rate was for

Model A0, at nearly 6%. For Models B and C, the percentage of improvement was medium between Models A and D, as shown in Figure 5.2.

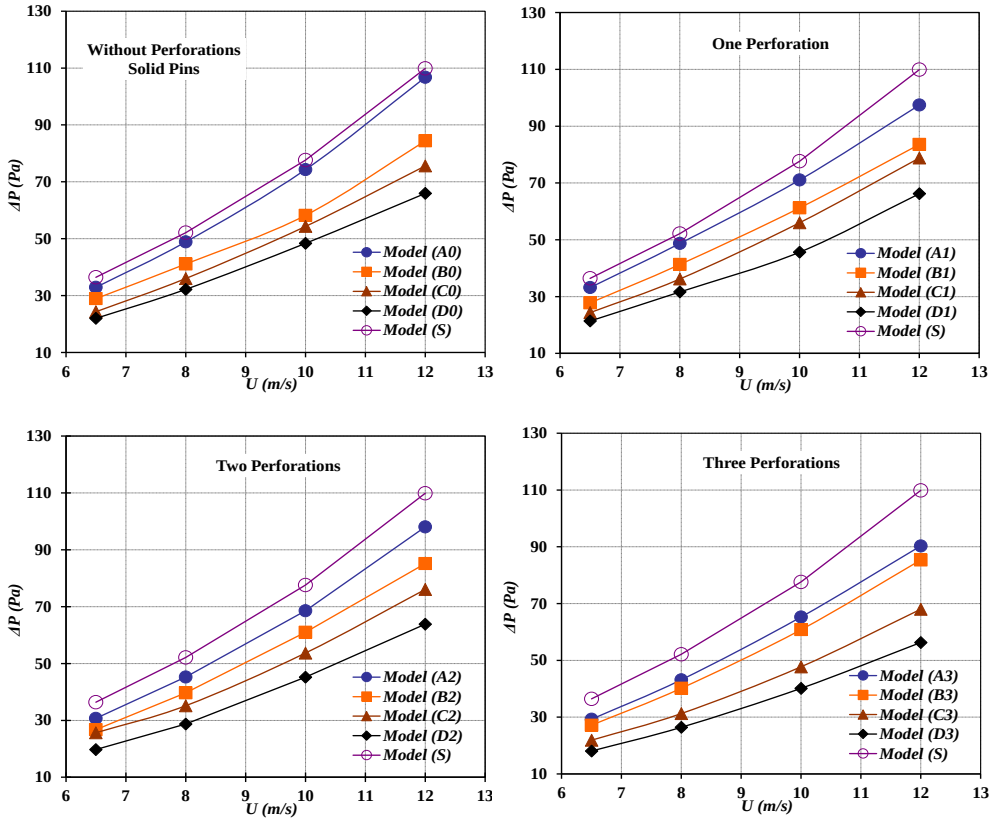

Figure 5.2. Comparison of pressure drops for different perforation numbers and cone inclination angles.

5.4. COMPARISON OF BASE TEMPERATURE FOR DIFFERENT PERFORATION NUMBERS AND CONE INCLINATION ANGLES

The main role of heat sinks in an electronic system is to maintain safe operating temperatures for the CPU in order to avoid failure and damage. According to [51], the most dangerous temperature for PCs is around 85°C. Figure 5.3 shows a decrease in the heat sink temperature when the velocity of airflow inside the test channel is increased with the temperature also decreasing when the number of holes for the conical pins increases, while the base temperature increases as the angle of inclination of the cone increases, due to the reasons mentioned earlier. This indicates that the increased heat transfer rates of the perforated conical pins have the desired impact of lowering the temperature of the heat sink. Thus, Models A2 and A3

achieve the preferred percentage of base temperature improvement at 5% and 4%, respectively, while Models C and D did not improve the core temperature.

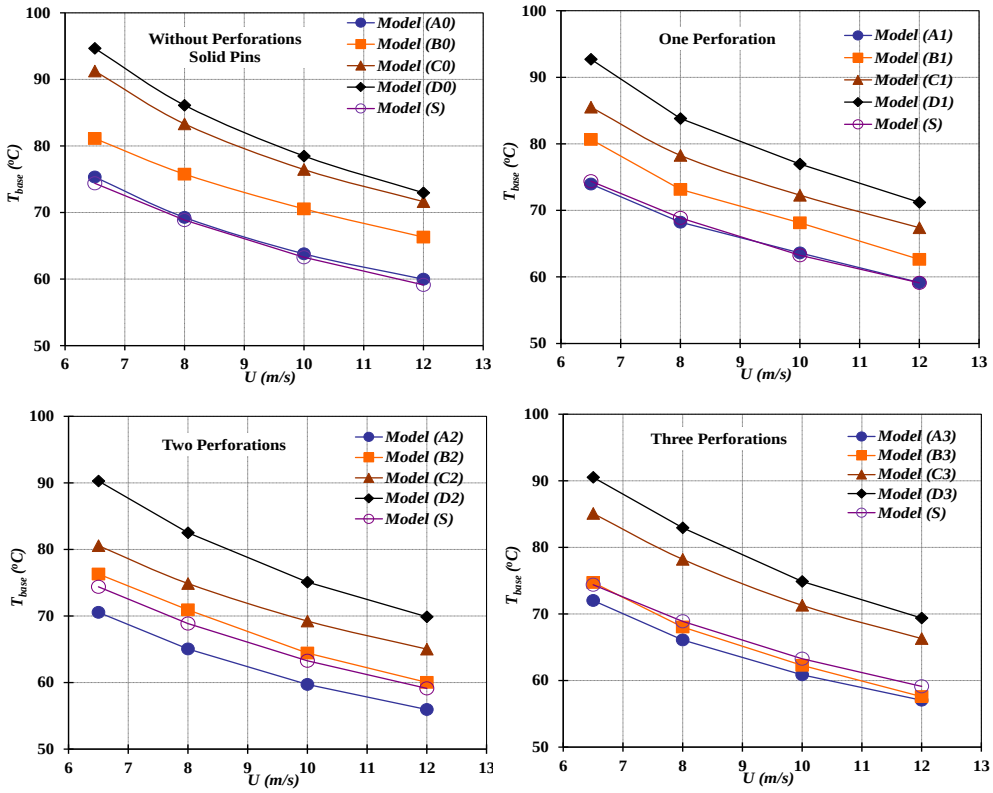

Figure 5.3. Comparison of base temperatures for different perforation numbers and cone inclination angles.

5.5. THE DESIRED MODEL

To select the desired model based on the evaluation of thermal and hydraulic characteristics of heat sinks, a precise formula of hydrothermal performance (HTP) should be followed. Hydrothermal performance (HTP) is calculated according to the following equation:

$$HTP = \left(\frac{Nu}{Nuo}\right)\left(\frac{\Delta Po}{\Delta P}\right)^{\frac{1}{3}} \tag{5.1}$$

where Nu_o and ΔP_o are the average Nu and ΔP for Model S, while Nu and ΔP are the average Nu and ΔP for the studied models. Figure 5.4 shows that the favorite model is Model B3 compared to other models. The highest value of HTP is nearly 1.15 at

U = 10m/s. This is due to the heat transfer improvement relative to the average Nu exceeding the increase in the pressure drop across the heat sinks.

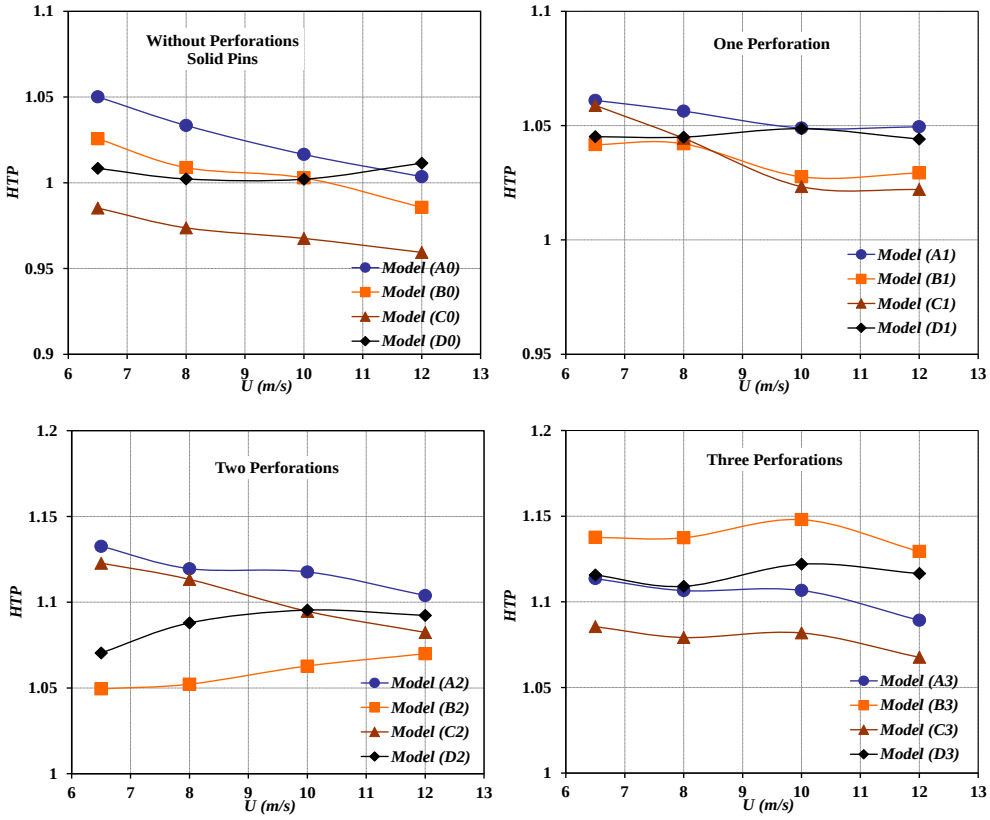

Figure 5.4. Comparison of HTP for different models.

5.6. TEMPERATURE AND FLOW CONTOURS

5.6.1. Influence of Perforations on The Flow and Temperature Fields

We can observe that the greater the number of holes, the greater the airflow pass through the perforations and a greater heat exchange is produced between the pins and the fluid. Therefore, the number of holes has a positive effect on reducing heat, as shown in Figure 5.5. This is mainly due to the fact that the number of holes is inversely proportional to ΔP and directly proportional to Nu.

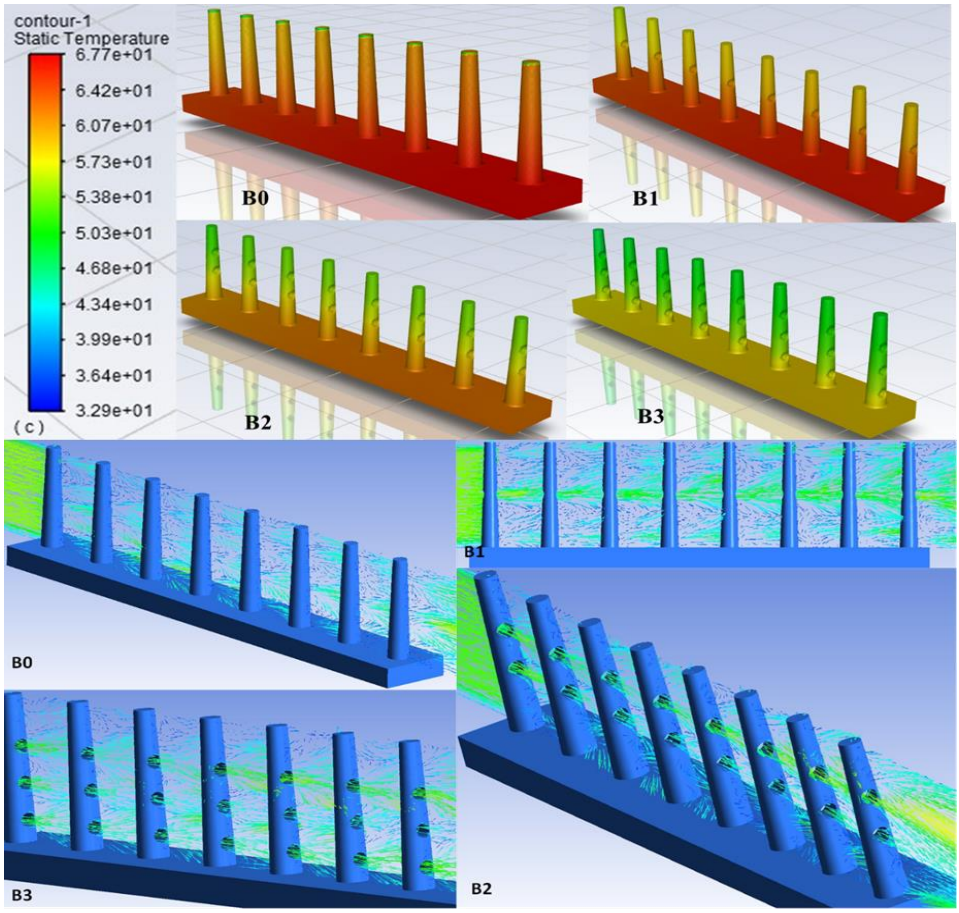

Figure 5.5. Influence of perforations on flow and temperature fields.

5.6.2. Influence of Angle of Inclination of Cones on Flow and Temperature Fields

Figure 5.6 shows that with the increase in the inclination angle of the conical pins, the less the surface is in contact with the airflow, so the models with the lowest inclination angle have a low temperature. Furthermore, the contact of the air flowing at a certain speed with the conical pins has two effects, the first of which is positive such that ΔP decreases as the inclination angle of the cone increases. The second effect is negative such that the heat exchange is low because the surface in contact with the air is less as the inclination angle of the cone increases. This leads to reductions in ΔP and Nu with increases in the angle of inclination of the cone.

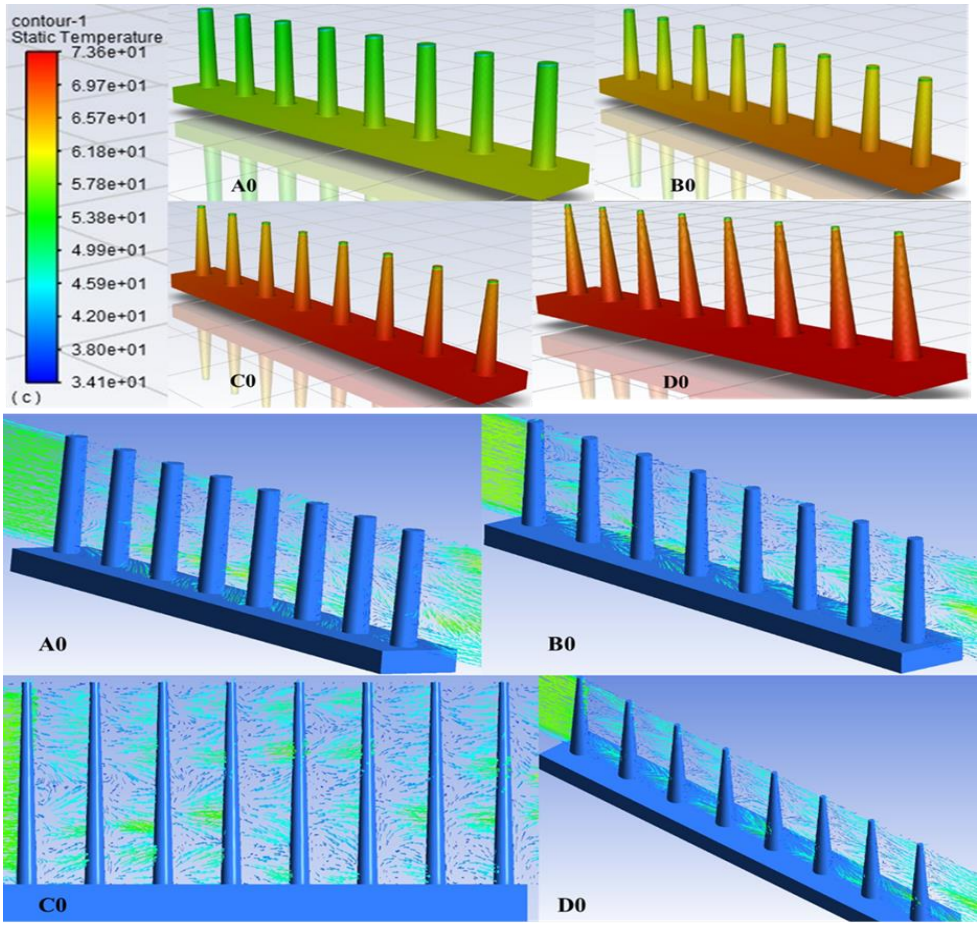

Figure 5.6 Influence of the angle of inclination of the cone on the flow and temperature fields.

5.7. COMPARISON OF CURRENT RESULTS WITH PREVIOUS RESEARCH

The comparison shows the advantages and disadvantages, and the similarity of the results of this study with previous studies. It used Model B3 in the comparisons as its values are balanced and average among the remainder of the models in the current study. Three studies are used in the comparison, the first is [23], presenting a fin circular shape solid, and perforated fin with three holes. The second is [30], presenting a fin circular shape solid, and perforated fin with three holes. The third is the model of [48], which is compared with three main variables: Nusselt number, which is the amount of heat exchanged, pressure drops, which represents energy being consumed, and the base temperature, through which it can keep the heat sink from reaching its thermal limit.

5.7.1. Nusselt Number

It can be observed that Model B3 in the current study that the Nusselt number is better by 19.8% than the model of [48] and almost equal (differing by 1.3%) to the model for solid fin for [23] and close to the model for perforated fin for [23] by 12%, as in Figure 5.7.

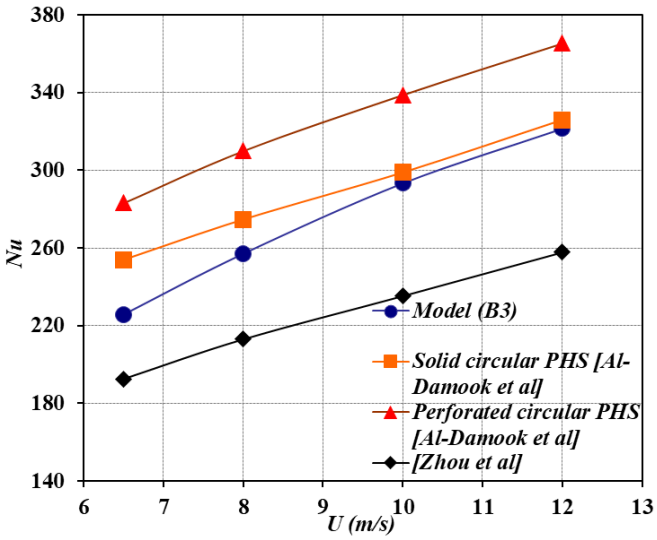

Figure 5.7. Comparison of Nusselt numbers.

5.7.2. Base Temperature

It is observed that the base temperature for Model B3 in the current study is better by 13.1% and 6.1%, respectively, than the solid and perforated models of [23], and better by 0.35% than the model for the solid fin for [30] and by 6.2% close to the model for the perforated fin for [30], as shown in Figure 5.8.

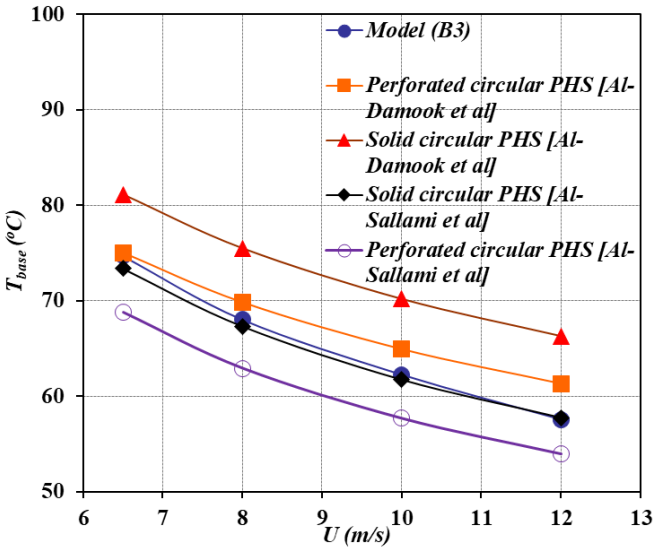

Figure 5.8. Comparison of base temperatures.

5.7.3. Pressure Drop

It can be observed that Model B3 in the current study outperformed all the models of previous studies, such that the pressure drop was 23.81% less than the model of [48], and 21.78% and 8.97% less, respectively, in the solid and perforated fins of the model of [23]. The models of [30] in the solid and perforated fin were exceeded by our model by 18.4% and 10.56%, respectively (Figure 5.9).

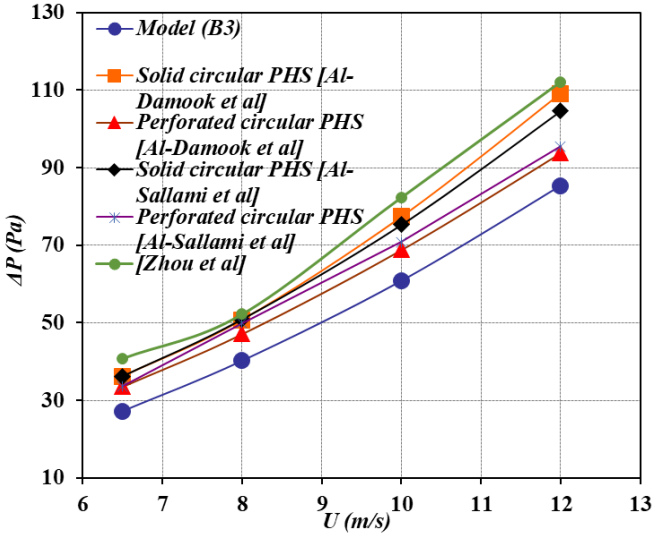

Figure 5.9. Comparison of pressure drops.

5.6. HEAT SINK MASS

Heat sink models are made as light as possible to conserve materials and improve portability while meeting their functional reduction in pressure drop and improvement in heat transfer requirements. Equations 5.2, 5.3 and 5.4 were used to determine the total mass of the heat sinks that were taken into consideration. Moreover, an aluminium density of 2,712 kg/m^3 is used in the calculation. The results presented in Table 5.1 show that the lowest reduction in mass is over 18% for heat sink Model D.

$$V_t = V_{base} + V_{pins} \tag{5.2}$$

$$m_t = \rho_{Al} . V_t \tag{5.3}$$

$$Reduction\ \% = (Model\ S - Three\ Perforations\ Model)/Model\ S \tag{5.4}$$

Table 5.1. Masses of the heat sink models.

Model	Mass of solid geometry (g)	Mass of one perforation geometry (g)	Mass of two perforations geometry (g)	Mass of three perforations geometry (g)	Reduction percentage (Model S - three perforations Model)/ Model S
Model S	19.01	-----	-----	-----	0%
Model A	18.12	17.88	17.64	17.38	8.57%
Model B	17.33	17.12	16.91	16.66	12.36%
Model C	16.65	16.47	16.28	16.04	15.62%
Model D	16.09	15.93	15.77	15.46	18.67%

PART 6

CONCLUSION AND RECOMMENDATIONS

6.1. CONCLUSION

Researchers have devoted considerable effort over the past few decades to enhancing the thermal efficiency of heat sinks while simultaneously reducing their size and improving the heat power output of electronic devices. This study examines four models of conical pin heat sinks, each inclined at a specific angle (A = 1°, B = 2°, C = 3° and D = 4°). Additionally, each conical pin design incorporates multiple perforations (N = 0, 1, 2, and 3). The investigation assesses the influence of a perforated conical pin and cone inclination angle on heat transfer, pressure drop (Δp), CPU temperature, and hydrothermal performance across the heat sinks using a 3D, turbulent flow, and heat transfer conjugate model. Consequently, we can conclude the following:

- Models D3 and C3 exhibit maximum reductions in pressure drop of approximately 49% and 23% respectively, while Model A0 shows a minimal reduction rate of nearly 6%.
- Model A2 achieved the highest rate of improvement in Nusselt number, with an increase of approximately 7%, followed by Model B3 with a rate of improvement of nearly 4%.
- Models A2 and A3 showed desirable reductions in base temperature of almost 5% and 4%, respectively.
- The Model D heat sink showcases a minimum reduction in mass of over 18%.
- The peak value of HTP, reaching approximately 1.15 at U = 10m/s, is observed in Model B3.

The perforated conical pin heat sink, therefore has the potential to achieve the primary objective of this study, namely superior heat transfer rate, pressure drop, base temperature, and mass reduction characteristics.

6.2. RECOMMENDATIONS FOR FUTURE WORK

This study presents a wide range of suggestions and recommendations for future studies as an extension of the current study.

- Studying the shapes of different pins, such as twisted, cylinder of different dimensions, and rhombic.
- Replacing the fluid coolant with water or nanofluids to absorb more heat.
- Changing the shape of the holes and making them square or rectangular.
- Checking the different arrangements of pins on the heat sink.
- Changing the type of flow by changing the ranges of Reynolds numbers.

REFERENCES

1. Zeadally, S., Khan, S. U., and Chilamkurti, N., "Energy-efficient networking: Past, present, and future", ***Journal Of Supercomputing***, 62 (3): 1093–1118 (2012).

2. Pan, Y., Yin, R., and Huang, Z., "Energy modeling of two office buildings with data center for green building design", ***Energy And Buildings***, 40 (7): 1145–1152 (2008).

3. Dai, J., Ohadi, M. M., Das, D., & Pecht, M. G. "Optimum cooling of data centers". ***New York (NY): Springer***, (2014).

4. Amip and Shah, "Thermal and Thermomechanical Phenomena in Electronic Systems, 2008, ITHERM 2008, 11th Intersociety Conference on : Date, 28-31 May 2008.", ***[IEEE]***, (2008).

5. Greenberg, S., Mills, E., Tschudi, B., Rumsey, P., & Myatt, B. "Best practices for data centers: Lessons learned from benchmarking 22 data centers". Proceedings of the ACEEE summer study on energy efficiency in buildings in Asilomar, CA. ***ACEEE***, August, 3, 76-87 (2006).

6. Al-damook, A. J. S. "Design optimisation and analysis of heat sinks for electronic cooling" ***(Doctoral dissertation, University of Leeds)***, (2016).

7. Gurrum, S. P., Suman, S. K., Joshi, Y. K., & Fedorov, A. G. "Thermal issues in next-generation integrated circuits". ***IEEE*** Transactions on device and materials reliability, 4(4), 709-714, (2004).

8. Mostafavi, G., "Natural Convective Heat Transfer from Interrupted Rectangular Fins", (2012).

9. Sette, B. The new European test and classification system for reaction to fire and resistance to fire. In Recent Advances on Flame Retardancy of Polymeric Materials Volume X. Proceedings of the 1999 BBC Conf., ***Business Communications Company Inc. Norwalk***, 1999, ISBN 156965-660-6 (pp. 389-401), (1999).

10. Chingulpitak, S., & Wongwises, S. "A review of the effect of flow directions and behaviors on the thermal performance of conventional heat sinks". ***International Journal of Heat and Mass Transfer***, 81, 10-18, (2015).

11. He, Z., Yan, Y., and Zhang, Z., "Thermal management and temperature uniformity enhancement of electronic devices by micro heat sinks: A review", ***Energy***, 216: (2021).

12. Soodphakdee, D., Behnia, M., & Copeland, D. W. “A comparison of fin geometries for heatsinks in laminar forced convection: Part I-round, elliptical, and plate fins in staggered and in-line configurations”. ***The International Journal of Microcircuits and Electronic Packaging,*** 24(1), 68-76, (2001).

13. Naphon, P. and Khonseur, O., “Study on the convective heat transfer and pressure drop in the micro-channel heat sink”, ***International Communications In Heat And Mass Transfer***, 36 (1): 39–44 (2009).

14. Brigham, B. A. and Vanfossen, G. J., “Length to Diameter Ratio and Row Number Effects in Short Pin Fin Heat Transfer”, (1984).

15. Dhumne, A. B. and Farkade, H. S., “Heat Transfer Analysis of Cylindrical Perforated Fins in Staggered Arrangement”, (2013).

16. Sahin, B. and Demir, A., “Thermal performance analysis and optimum design parameters of heat exchanger having perforated pin fins”, ***Energy Conversion And Management***, 49 (6): 1684–1695 (2008).

17. Sahin, B. and Demir, A., “Performance analysis of a heat exchanger having perforated square fins”, ***Applied Thermal Engineering***, 28 (5–6): 621–632 (2008).

18. Diani, A., Mancin, S., Zilio, C., and Rossetto, L., “An assessment on air forced convection on extended surfaces: Experimental results and numerical modeling”, ***International Journal Of Thermal Sciences***, 67: 120–134 (2013).

19. Yakut, K., Alemdaroglu, N., Kotcioglu, I., and Celik, C., “Experimental investigation of thermal resistance of a heat sink with hexagonal fins”, ***Applied Thermal Engineering***, 26 (17–18): 2262–2271 (2006).

20. Wang, G., Niu, D., Xie, F., Wang, Y., Zhao, X., and Ding, G., “Experimental and numerical investigation of a microchannel heat sink (MCHS) with micro-scale ribs and grooves for chip cooling”, ***Applied Thermal Engineering***, 85: 61–70 (2015).

21. Khan, J., Momin, S. A., & Mariatti, M. “A review on advanced carbon-based thermal interface materials for electronic devices”. ***Carbon***, 168, 65-112, (2020).

22. Jonsson, H., & Moshfegh, B. “Modeling of the thermal and hydraulic performance of plate fin, strip fin, and pin fin heat sinks-influence of flow bypass”. ***IEEE*** Transactions on Components and Packaging Technologies, 24(2), 142-149, (2001).

23. Al-Damook, A., Kapur, N., Summers, J. L., and Thompson, H. M., “Computational design and optimisation of pin fin heat sinks with rectangular perforations”, ***Applied Thermal Engineering***, 105: 691–703 (2016).

24. Agostinis, P., Berg, K., Cengel, K. A., Foster, T. H., Girotti, A. W., Gollnick, S. O., ... & Golab, J. "Photodynamic therapy of cancer: an update". CA: ***a cancer journal for clinicians***, 61(4), 250-281 (2011).

25. ALGBURI, N. I. H. "NUMERICAL ANALYSIS OF EFFECTS OF THE TWISTING ANGLE ON THERMOHYDRAULIC PERFORMANCE OF A HEXAGONAL PIN FIN ARRAY" ***(Doctoral dissertation)***, (2022).

26. Choudhary, V., Kumar, M., and Patil, A. K., "Experimental investigation of enhanced performance of pin fin heat sink with wings", ***Applied Thermal Engineering***, 155: 546–562 (2019).

27. Journal, I., Hatem, M., Abdellatif, H., and Hussein, W., "IRJET-Enhancement of Perforated Pin-Fins Heat Sink under Forced Convection Cite this paper Enhancement of Perforated Pin-Fins Heat Sink under Forced Convection", ***International Research Journal Of Engineering And Technology***, (2020).

28. Srikanth, R. and Balaji, C., "Experimental investigation on the heat transfer performance of a PCM based pin fin heat sink with discrete heating", ***International Journal Of Thermal Sciences***, 111: 188–203 (2017).

29. Bakhti, F. Z. and Si-Ameur, M., "A comparison of mixed convective heat transfer performance of nanofluids cooled heat sink with circular perforated pin fin", ***Applied Thermal Engineering***, 159: (2019).

30. Al-Sallami, W., Al-Damook, A., and Thompson, H. M., "A numerical investigation of thermal airflows over strip fin heat sinks", ***International Communications In Heat And Mass Transfer***, 75: 183–191 (2016).

31. Gupta, D., Saha, P., and Roy, S., "Computational analysis of perforation effect on the thermo-hydraulic performance of micro pin-fin heat sink", ***International Journal Of Thermal Sciences***, 163: (2021).

32. Sahel, D., Bellahcene, L., Yousfi, A., and Subasi, A., "Numerical investigation and optimization of a heat sink having hemispherical pin fins", ***International Communications In Heat And Mass Transfer***, 122: (2021).

33. Maji, A., Bhanja, D., & Patowari, P. K. "Computational investigation and optimisation study on system performance of heat sink using perforated pin fins mounted at different angles". *Progress in Computational Fluid Dynamics, **An International Journal***, *19*(6), 381-400, (2019).

34. Ghyadh, N. A., Ahmed, S. S., & Al-Baghdadi, M. A. R. S. Enhancement of forced convection heat transfer from cylindrical perforated fins heat sink-CFD study. ***Journal of Mechanical Engineering Research and Developments***, 44(3), 407-419 (2021).

35. Mandal, P. K., Sengupta, S., Rana, S. C., & Bhanja, D. "Effect of orientation angle in thermal performance analysis of a horizontal heat sink of perforated pin fins". In AIP Conference Proceedings (Vol. 2148, No. 1). ***AIP Publishing***, (2019, September).

36. Alfellag, M. A., Ahmed, H. E., and Kherbeet, A. S., "Numerical simulation of hydrothermal performance of minichannel heat sink using inclined slotted plate-fins and triangular pins", ***Applied Thermal Engineering***, 164: (2020).

37. Haque, M. R., Hridi, T. J., and Haque, M. M., "CFD studies on thermal performance augmentation of heat sink using perforated twisted, and grooved pin fins", ***International Journal Of Thermal Sciences***, 182: (2022).

38. Ahmadian-Elmi, M., Mashayekhi, A., Nourazar, S. S., and Vafai, K., "A comprehensive study on parametric optimization of the pin-fin heat sink to improve its thermal and hydraulic characteristics", ***International Journal Of Heat And Mass Transfer***, 180: (2021).

39. Huang, C. H. and Huang, Y. R., "An optimum design problem in estimating the shape of perforated pins and splitters in a plate-pin-fin heat sink", ***International Journal Of Thermal Sciences***, 170: (2021).

40. Khattak, Z., & Ali, H. M. Air cooled heat sink geometries subjected to forced flow: A critical review. ***International Journal of Heat and Mass Transfer***, *130*, 141-16 (2019).

41. Baldry, M., Timchenko, V., and Menictas, C., "Optimal design of a natural convection heat sink for small thermoelectric cooling modules", ***Applied Thermal Engineering***, 160: (2019).

42. Tariq, A., Altaf, K., Ahmad, S. W., Hussain, G., and Ratlamwala, T. A. H., "Comparative numerical and experimental analysis of thermal and hydraulic performance of improved plate fin heat sinks", ***Applied Thermal Engineering***, 182: (2021).

43. Song, G., Kim, D. H., Song, D. H., Sung, J. Bin, and Yook, S. J., "Heat-dissipation performance of cylindrical heat sink with perforated fins", ***International Journal Of Thermal Sciences***, 170: (2021).

44. Towsyfyan, H., Freegah, B., Hussain, A. A., and El-Deen Faik, A. M., "Novel design to enhance the thermal performance of plate-fin heat sinks based on CFD and artificial neural networks", ***Applied Thermal Engineering***, 219: (2023).

45. Abuşka, M. and Çorumlu, V., "A comparative experimental thermal performance analysis of conical pin fin heat sink with staggered and modified staggered layout under forced convection", ***Thermal Science And Engineering Progress***, 37: (2023).

46. Anandan, S.S., & Ramalingam, V. Thermal management of electronics: A review of literature. ***Thermal Science***, *12*, 5-26 (2008).

47. Kraus, A. D., Aziz, A., and Welty, J., "Frontmatter", Extended Surface Heat Transfer, ***John Wiley & Sons, Inc.***, I–XIV (2007).

48. Zhou, F. and Catton, I., “Numerical evaluation of flow and heat transfer in plate-pin fin heat sinks with various pin cross-sections”, ***Numerical Heat Transfer; Part A: Applications***, 60 (2): 107–128 (2011).

49. Ventola, L., Chiavazzo, E., Calignano, F., Manfredi, D., & Asinari, P. “Heat transfer enhancement by finned heat sinks with micro-structured roughness”. ***In Journal of Physics:*** Conference Series (Vol. 494, No. 1, p. 012009). IOP Publishing, (2014, April).

50. Shaeri, M. R., & Jen, T. C. “The effects of perforation sizes on laminar heat transfer characteristics of an array of perforated fins”. ***Energy Conversion and Management***, 64, 328-334, (2012).

51. Yuan, W., Zhao, J., Tso, C. P., Wu, T., Liu, W., and Ming, T., “Numerical simulation of the thermal hydraulic performance of a plate pin fin heat sink”, ***Applied Thermal Engineering***, 48: 81–88 (2012).

RESUME

Mohammed Ahmed Al-KAROOSHİ, a mechanical engineer, graduated from the College of Engineering, Al Anbar University, and obtained a bachelor’s degree in 2020. He is currently studying for a master’s degree at Karabük University in mechanical engineering.